

# ENTROPY BOUNDS FOR GLASS NETWORKS

BENJAMIN W. WILD\* AND RODERICK EDWARDS†

**Abstract.** We propose that chaotic Glass networks (a class of piecewise-linear Ordinary Differential Equations) are good candidates for the design of true random number generators. A Glass network design has the advantage of involving only standard Boolean logic gates. Furthermore, an already chaotic (deterministic) system combined with random “jitter” due to thermal noise can be used to generate random bit sequences in a more robust way than noisy limit-cycle oscillators. Since the goal is to generate bit sequences with as large a positive entropy as possible, it is desirable to have a theoretical method to assess the irregularity of a large class of networks. We develop a procedure here to calculate good upper bounds on the entropy of a Glass network, by means of symbolic representations of the continuous dynamics. Our method improves on a result by Farcot (2006), and allows in principle for an arbitrary level of precision by refinements of the estimate, and we show that in the limiting case, these estimates converge to the true entropy of the symbolic system corresponding to the continuous dynamics. As a check on the method, we demonstrate for an example network that our upper bound after only a few refinement steps is very close to the entropy estimated from a long numerical simulation.

**Key words.** Glass networks, entropy, symbolic dynamics, chaos, piecewise smooth ODEs, dynamical systems, true random number generators

**MSC codes.** 34A36, 34C28, 37B10, 37B40, 94C99

**1. Introduction.** A number of designs for intrinsically chaotic free-running electronic circuits have been described, most famously the Chua circuit [14, 26, 32], but other designs [4, 24, 34, 38] have been proposed. Some of these may be good choices for designs of both Pseudo-Random Number Generators (PNRGs) and True Random Number Generators (TRNGs). While TRNGs, unlike PRNGs, depend on the thermal noise always present in electronic circuits to randomly perturb their dynamics and thus allow the extraction of random bit sequences, designs based on limit cycle oscillators [23, 36] are subject to hacking, by, for example, frequency injection attack [2, 30] or other methods [31]. A circuit that would display chaotic behaviour even in the absence of thermal noise makes entrainment more difficult, and thus makes it more difficult for a hacker to disrupt security by eliminating or reducing the randomness.

A number of circuit designs have been proposed to implement this idea [5, 25, 34, 35, 37]. The design proposed in [12] has the advantage of using only standard Boolean logic gates, which also means that it can be described by a Glass network. Indeed, a class of possible designs for random number generation are Glass networks that have already been shown to be chaotic, or at least to have an aperiodic attractor. Glass networks are a class of piecewise-linear systems of ordinary differential equations (ODEs), which were originally proposed as qualitative models of gene regulation [9, 16, 17, 18, 19, 20, 21], but have also been implemented in electronic circuitry [12, 22, 29] where the sharpness of the switching between high and low states makes the model a more accurate approximation of such circuit behaviour than of typical gene networks where switching may not be so steep. Demonstration of chaotic, or at least aperiodic behaviour in low-dimensional examples of such networks has been shown in several ways [6, 7, 8, 27, 33].

Entropy is one measure of randomness in a chaotic dynamical system [1]. It is

---

\*Dept. of Mathematics and Statistics, University of Victoria, P.O. Box 1700 STN CSC, Victoria, B.C., Canada, V8W 2Y2 ([benwwild@uvic.ca](mailto:benwwild@uvic.ca)).

†Dept. of Mathematics and Statistics, University of Victoria, P.O. Box 1700 STN CSC, Victoria, B.C., Canada, V8W 2Y2 ([edwards@uvic.ca](mailto:edwards@uvic.ca)).

particularly relevant in the context of TRNGs, since the objective in that situation is to generate sequences of bits with positive entropy. For Glass networks, entropy estimates have been discussed by Glass et al. [10] and more rigorously by Farcot [11]. Farcot obtains an upper bound on entropy of the dynamics of a Glass network, by means of the entropy of a Transition Graph (TG) associated with the equations. The TG captures the transitions between states (rectangular regions of phase space, called *boxes*) that are allowed by the structure of the equations. The topological entropy of this TG is shown, using a corresponding symbolic dynamics, to be an upper bound for the actual dynamics of the network. However, it is often not a very sharp upper bound, since the TG typically allows a great many more transitions than actually occur in a trajectory of the differential equations, especially if the latter is restricted to an attractor (*i.e.*, ignoring any transient behaviour), which is the pertinent object for the behaviour of a circuit acting as a TRNG.

Here we show how Farcot’s approach to producing an upper bound on entropy for a Glass network can be improved, in some cases dramatically improved, by taking into consideration more information about the actual dynamics of the network. As a first step, the TG can be pruned to remove transitions that do not occur on the attractor of interest. Periodic attractors in Glass networks can often be identified directly, and proven to exist and to be asymptotically attracting. Of course, they must have zero entropy, but one can also sometimes prove that no such stable periodic orbit exists. A trapping region on a *wall* between boxes, serving as a Poincaré section, can often be identified, even when there is no stable periodic orbit, which restricts trajectories to a certain subgraph of the TG. Furthermore, it is often possible to refine the entropy estimate further by identifying sequences of cycles on the Poincaré section that do not occur, and thus correspond to forbidden blocks in the corresponding symbolic dynamics. We use a particular Glass network as a test example throughout, but the methodology is applicable to the entire class of networks considered.

In Section 2, we introduce briefly Glass networks and the analysis of their dynamics, mainly following the notation of Farcot [11]. In Section 3 we outline Farcot’s proof that the entropy of the TG is an upper bound for the entropy of the network dynamics. Then in Section 4 we adapt this approach to show how an improved upper bound may be obtained. In Section 5 we apply this analysis to a particular Glass network, and show how further refinements can be made in Section 6. Finally, in Section 7 we show by means of numerical simulations how much closer our upper bound is to numerical estimates of entropy than the entropy based on the entire TG.

**2. Glass Networks.** Glass networks are of the form

$$(2.1) \quad \dot{x} = -\Lambda x + \Gamma(x)$$

where  $x \in \mathbb{R}^n$ ,  $\Lambda \in \mathbb{R}^{n \times n}$  is a positive diagonal matrix with diagonal entries  $\lambda_i$ ,  $i = 1, \dots, n$ , and  $\Gamma : \mathbb{R}^n \rightarrow \mathbb{R}^n$  is constant on rectangular regions of phase space defined by thresholds, as detailed below. The following background on the structure and analysis of Glass networks closely follows Farcot [11] since this work builds upon what is discussed there.

Since  $\Gamma$  is bounded, the flow is also bounded. The dynamics of interest occur within the  $n$ -dimensional rectangular region

$$\mathcal{U} = \prod_{i=1}^n \left[ 0, \max_{x \in \mathbb{R}_+^n} \left\{ \frac{\Gamma_i(x)}{\lambda_i} \right\} \right],$$

which is positively invariant. The flow from any (non-negative) initial point outside

$\mathcal{U}$  must flow into it and cannot then escape. Note that in Farcot [11],  $\mathcal{U}$  is defined as  $[0, 1]^n$ , but this would only be true after a normalization that we do not make. Since  $\Lambda$  is a constant diagonal matrix, Equation (2.1) only describes systems with linear degradation rates. Thus, we do not here include systems with coupling in the degradation term.  $\mathcal{U}$  is partitioned by the discontinuities present in the coupling term,  $\Gamma(x)$ , which is constant on *boxes*,  $n$ -dimensional rectangular regions that are products of bounded intervals. Thus, in each box Equation (2.1) is a first order linear system.

The discontinuities of  $\Gamma$  define the boundaries between boxes in phase space, which are referred to as *walls*. The set of *threshold* values (discontinuities of  $\Gamma$ ) are denoted by  $\Theta_i = \{\theta_{i,j} | j \in \{1, \dots, p_i\}\}$  for each coordinate  $x_i$  of  $x$ . Like Farcot [11], we will assume that the sets  $\Theta_i$  are ordered  $\theta_{i,1} < \theta_{i,2} < \dots < \theta_{i,p_i}$ . Boxes can then be written as

$$(2.2) \quad B_a = B_{a_1 \dots a_n} = \prod_{i=1}^n [\theta_{i,a_i}, \theta_{i,a_i+1}]$$

where  $a$  belongs to the finite set

$$(2.3) \quad \mathcal{A} = \prod_{i=1}^n \{1, \dots, p_i\}.$$

Since the subscript  $a$  uniquely determines a box,  $\mathcal{A}$  defines an alphabet of symbols that will later be used in symbolic dynamical systems that qualitatively describe the dynamics of System (2.1). Since  $\Gamma$  is constant on a box, it will also be convenient later to consider the mapping  $\Gamma$  as  $\Gamma : \mathcal{A} \rightarrow \mathbb{R}^n$ . (While  $\Gamma$  should really be considered as the composition of a map from  $\mathbb{R}^n$  to  $\mathcal{A}$  and a map from  $\mathcal{A}$  to  $\mathbb{R}^n$ , it will not cause confusion to abuse notation and refer to the latter map as  $\Gamma$ .)

Equation (2.1) can be solved within a given box  $B_a$ , where  $\Gamma$  is a constant vector and the system is first order linear, to give:

$$(2.4) \quad x(t) = f + e^{-\Lambda t}(x(0) - f)$$

where  $f = [\gamma_1/\lambda_1, \dots, \gamma_n/\lambda_n]^\top$  is referred to as a focal point for the box  $B_a$ . The flow is clearly attracted towards  $f$  (in each variable). If  $f \in B_a$ ,  $f$  is an asymptotically stable steady state. Otherwise, before the trajectory can reach  $f$ , it will intersect a wall between  $B_a$  and another box. If the wall is crossed then  $\Gamma$  takes a new constant value (in general) and the trajectory continues. The boundary of  $B_a$  is formed by  $k$ -faces that are  $k$ -dimensional rectangles where  $k \in \{0, \dots, n-1\}$ . When the trajectory crosses an  $(n-1)$ -dimensional face (a wall) there is at most one adjacent box the trajectory can continue in, and so the value of  $\Gamma$  is unambiguous, unless the flow is towards the wall on both sides. In the latter case (a *black wall*), the wall is not crossed. Rather, the subsequent flow is constrained to the wall, and we need either Filippov theory for discontinuous systems, or singular perturbation theory to determine the flow. If the trajectory crosses a face that has dimension less than  $n-1$  there are several possible adjacent boxes that the trajectory could continue into, and again Filippov solutions or singular perturbation is sometimes required. Here, we will restrict the discussion to walls, *i.e.*, faces of dimension  $n-1$ , that are actually crossed. These are called *transparent* walls.

Continuous trajectories from wall crossing to wall crossing can be easily constructed, as long as walls are transparent. In order to ensure this, we will assume that the following two conditions are met.

**Condition 1.**  $\forall a \in \mathcal{A}, f(a) \in \bigcup_{a \in \mathcal{A}} \text{int}(B_a)$ .

Here  $f$  acts as the map  $\Lambda^{-1} \circ \Gamma : \mathcal{A} \rightarrow \mathbb{R}^n$  to give the focal point for the box  $B_a$ , and  $\text{int}(B_a)$  is the interior of  $B_a$ . This assumption ensures that no focal points are located on a box boundary.

**Condition 2.**  $\forall i \in \{1, \dots, n\}, \forall a, a' \in \mathcal{A}$  such that  $a - a' = \pm e_i$ , either

$$(\mathbf{d}_i(f(a)) - a_i) (\mathbf{d}_i(f(a')) - a'_i) > 0,$$

or

$$(\mathbf{d}_i(f(a)) - a_i) = 0 \quad \text{and} \quad (\mathbf{d}_i(f(a')) - a'_i) (a_i - a'_i) > 0$$

or

$$(\mathbf{d}_i(f(a')) - a'_i) = 0 \quad \text{and} \quad (\mathbf{d}_i(f(a)) - a_i) (a_i - a'_i) > 0$$

where  $e_i$  is the  $i^{\text{th}}$  basis vector in  $\mathbb{R}^n$  and  $\mathbf{d} = (\mathbf{d}_1, \dots, \mathbf{d}_n) : \bigcup_a \text{int}(B_a) \rightarrow \mathcal{A}$  is the discretizing operator, which maps a point lying inside a box to the subscript denoting the box.

This Condition ensures that the flow on both sides of a wall between adjacent boxes is in the same direction, so that black (or white) walls cannot occur. Boxes  $a$  and  $a'$  are adjacent in the  $x_i$  direction when  $a - a' = \pm e_i$ , and the flow direction in box  $a$  of variable  $x_i$  is determined by the sign of  $(\mathbf{d}_i(f(a)) - a_i)$ . In the context of gene regulation, Condition 2 is satisfied when there is no auto-regulation in the system.

Given a box  $B_a$  and the solution trajectory defined by Equation (2.4) within the box, if a wall is crossed, the time and position that the trajectory encounters the wall is easy to calculate. Which wall, if any, is encountered uniquely depends on the position of the focal point for the box. The wall  $\{x_i = \theta_{i,a_i}\}$  can be crossed if and only if  $f_i < \theta_{i,a_i}$  and the wall  $\{x_i = \theta_{i,a_i+1}\}$  can be crossed if and only if  $f_i > \theta_{i,a_i+1}$ . The set of possible output walls, either on the upper or lower side in each direction, is thus captured by

$$I_{\text{out}}^+(a) = \{i \in \{1, \dots, n\} | f_i > \theta_{i,a_i+1}\}$$

and

$$I_{\text{out}}^-(a) = \{i \in \{1, \dots, n\} | f_i < \theta_{i,a_i}\}$$

with

$$I_{\text{out}}(a) = I_{\text{out}}^+(a) \cup I_{\text{out}}^-(a)$$

Now for each direction in  $I_{\text{out}}(a)$ , the time it takes for  $x(t)$  to reach the threshold from an initial point,  $x_0$  according to the flow of  $B_a$  would be given by

$$\tau_i(x_0) = -\frac{1}{\lambda_i} \ln(\alpha_i^-(x_0)) \quad \text{if} \quad i \in I_{\text{out}}^-(a)$$

and

$$\tau_i(x) = -\frac{1}{\lambda_i} \ln(\alpha_i^+(x_0)) \quad \text{if} \quad i \in I_{\text{out}}^+(a)$$

where

$$\alpha_i^-(x) = \frac{f_i - \theta_{i,a_i}}{f_i - x_i} \quad \text{and} \quad \alpha_i^+(x) = \frac{f_i - \theta_{i,a_i+1}}{f_i - x_i}.$$

Finally, the time to encounter a wall from  $x \in B_a$  is given by

$$(2.5) \quad \tau(x_0) = \min_{i \in I_{\text{out}}(a)} \tau_i(x_0)$$

and putting this into Equation (2.4) gives the exit point of  $B_a$  from the initial condition  $x_0 \in B_a$ . The starting point of a trajectory can be chosen to be on a wall, and then the subsequent sequence of wall transitions can be calculated by repeating the above. It follows from Equation (2.4) and Equation (2.5) that the map from wall to wall is given by  $\mathcal{M}_a : \partial B_a \rightarrow \partial B_a$  where

$$(2.6) \quad \begin{aligned} \mathcal{M}_a x &= x(\tau(x_0)) \\ &= f + e^{-\Lambda\tau(x_0)}(x_0 - f). \end{aligned}$$

Within each box  $B_a$ ,  $I_{\text{out}}(a)$  determines all boxes that are reachable from  $B_a$ . These boxes are adjacent to  $B_a$  through walls supported by hyperplanes that take the form  $\{x_i = \theta_{i,j}\}$ , where  $i \in I_{\text{out}}$  and  $j \in \{a_i, a_i + 1\}$  depends on whether  $i$  belongs to  $I_{\text{out}}^-(a)$  or  $I_{\text{out}}^+(a)$ . Using that distinction, walls can be denoted as

$$W_i^+(a) = \{x | x_i = \theta_{i,a_i+1}\} \cap B_a$$

and

$$W_i^-(a) = \{x | x_i = \theta_{i,a_i}\} \cap B_a.$$

Each box can then be partitioned into regions associated with each element of  $I_{\text{out}}(a)$  where only a single adjacent box is reachable from each region. The only walls that trajectories can escape  $B_a$  by are then  $W_i^+(a)$  for  $i \in I_{\text{out}}^+(a)$ , and  $W_i^-(a)$  for  $i \in I_{\text{out}}^-(a)$ . So, given any initial condition  $x$ , the directions  $i$  such that  $\tau(x) = \tau_i(x)$  are those for which  $\mathcal{M}_a x \in W_i^\pm(a)$ . Normally there is only one such direction and a particular wall through which we exit  $B_a$ , but it is possible that multiple walls are reached simultaneously, in which case there is more than one such direction,  $i$ . Now  $\partial B_a$  can be partitioned into two regions:

$$\partial B_a^{\text{out}} = \bigcup_{i \in I_{\text{out}}^\pm(a)} W_i^\pm(a) = \{x \in B_a | \tau(x) = 0\}$$

(points on the boundary of  $B_a$  from which it takes no time at all to exit, *i.e.*, exit walls), and

$$\partial B_a^{\text{in}} = \overline{\partial B_a} \setminus \overline{\partial B_a^{\text{out}}} = \bigcup_{i \in I_{\text{out}}^\pm(a)} W_i^\mp(a) \cup \bigcup_{i \notin I_{\text{out}}(a)} (W_i^-(a) \cup W_i^+(a)),$$

where  $\mp$  in each case indicates the opposite sign to  $\pm$ . Thus, the incoming and outgoing regions are unions of walls, which are closed and cover the boundary of  $\partial B_a$ . It then follows that  $\partial B_a^{\text{out}} \cap \partial B_a^{\text{in}} \neq \emptyset$  whenever  $\partial B_a^{\text{out}} \neq \emptyset$ , since it includes some threshold intersections. Under **Condition 1**, it always holds that  $\partial B_a^{\text{in}} \neq \emptyset$  because

$i \in I_{\text{out}}^{\pm}(a) \Rightarrow W_i(a)^{\mp} \subset \partial B_a^{\text{in}}$ , and  $i \notin I_{\text{out}}(a) \Rightarrow W_i^-(a) \cup W_i^+(a) \subset \partial B_a^{\text{in}}$ . This first partition of the boundary of  $B_a$  only allows for a distinction to be made between exit directions and the others. It follows that  $\partial B_a^{\text{out}} = \emptyset$  if and only if  $f \in \text{int}(B_a)$ .

Using this partition, it is proven by Farcot [11] that under the assumptions of **Condition 1** and provided  $\partial B_a^{\text{out}} \neq \emptyset$ , when  $\mathcal{M}_a$  is restricted to the domain and range  $\partial B_a^{\text{in}}$  and  $\partial B_a^{\text{out}}$  respectively,  $\mathcal{M}_a$  is a homeomorphism.

Now for a box  $B_a$ , escaping walls are of the form  $W_j^{\pm}(a)$ , for  $j \in I_{\text{out}}(a)$ , where  $\pm$  has a fixed value for each  $j$ . So in accordance with Farcot [11],  $\pm_j = \text{sign}(\mathbf{d}_j(f(a)) - a_j)$  will denote the unique sign for each  $j$  such that  $j \in I_{\text{out}}^{\pm_j}(a)$ , and again  $\mp_j$  is the opposite of  $\pm_j$ . Now, for  $i \in I_{\text{out}}(a)$ , define  $\theta_{i,a_i}^{\pm}$  as the threshold value that can be reached in the direction  $i$ , where  $\theta_{i,a_i}^- = \theta_{i,a_i}$  and  $\theta_{i,a_i}^+ = \theta_{i,a_i+1}$ . Then, domains and ranges for  $\mathcal{M}_a$  can be explicitly written as

$$(2.7) \quad \begin{aligned} D_{i,j}^{\pm}(a) &= W_i^{\pm}(a) \cap \mathcal{M}_a^{-1}(W_j^{\pm_j}(a)) \text{ for } i \in \{1, \dots, n\} \setminus I_{\text{out}}(a), j \in I_{\text{out}}(a) \\ D_{i,j}(a) &= W_i^{\mp_i}(a) \cap \mathcal{M}_a^{-1}(W_j^{\pm_j}(a)) \text{ for } i, j \in I_{\text{out}}(a) \end{aligned}$$

and

$$(2.8) \quad \begin{aligned} R_{i,j}^{\pm}(a) &= \mathcal{M}_a(W_i^{\pm}(a)) \cap W_j^{\pm_j} \text{ for } i \in \{1, \dots, n\} \setminus I_{\text{out}}(a), j \in I_{\text{out}}(a) \\ R_{i,j}(a) &= \mathcal{M}_a(W_i^{\mp_i}(a)) \cap W_j^{\pm_j} \text{ for } i, j \in I_{\text{out}}(a) \end{aligned}$$

In the definitions of  $D_{i,j}^{\pm}$  and  $R_{i,j}^{\pm}$ , two sets are defined in each case, one with the  $+$  sign and one with the  $-$  sign, since when  $i \notin I_{\text{out}}(a)$  both of the walls  $W_i^+(a)$  and  $W_i^-(a)$  are subsets of  $\partial B_a^{\text{in}}$ . However, for  $i \in I_{\text{out}}(a)$  it is always the case that  $W_i^{\pm_i}(a) \subset \partial B_a^{\text{out}}$  and  $W_i^{\mp_i}(a) \subset \partial B_a^{\text{in}}$ . The fact that these sets partition  $\partial B_a$  follows from the fact that  $\mathcal{M}_a$  is a homeomorphism, and thus a bijection. Each point on a wall  $W_i^{\pm}(a) \subset \partial B_a^{\text{in}}$  must be mapped to a wall in  $\partial B_a^{\text{out}}$  of the form  $W_j^{\pm_j}(a)$ . Hence  $D_{i,j}^{\pm}(a)$  and  $D_{i,j}(a)$  partition  $\partial B_a^{\text{in}}$ . Similarly,  $\partial B_a^{\text{out}}$  is partitioned by the sets  $R_{i,j}^{\pm}(a)$  and  $R_{i,j}(a)$ . In fact, it is shown by Farcot [11] that

$$\begin{aligned} R_{i,j}^{\pm}(a) &= \mathcal{M}_a(D_{i,j}^{\pm}(a)) \text{ for } i \in \{1, \dots, n\} \setminus I_{\text{out}}(a), j \in I_{\text{out}}(a), \\ R_{i,j}(a) &= \mathcal{M}_a(D_{i,j}(a)) \text{ for } i, j \in I_{\text{out}}(a). \end{aligned}$$

Farcot [11], in his Propositions 4 and 5, shows that the sets  $D_{i,j}^{\pm}(a)$  and  $D_{i,j}(a)$ ,  $R_{i,j}^{\pm}(a)$  and  $R_{i,j}(a)$  are bounded cells with piecewise smooth boundaries that can be explicitly given in terms of inequalities.

It is pointed out by Farcot that in the case where all  $\lambda_i$  are equal, all the inequalities that define the domains and ranges of the map  $\mathcal{M}_a$  through a box  $B_a$  are affine, so that the regions are polytopes. In the examples we investigate later, this will be the case.

Previously the transition mapping  $\mathcal{M}_a$  was rigorously defined as a homeomorphism within the confines of a single box. Now we turn our attention to transitions maps on the whole state space. Although maps defined within boxes with nonempty outgoing domains are invertible, boxes with no escaping direction are more problematic. It is natural to map the boundary of these types of boxes to a single point whose pre-image is the entire box boundary. As a result, in general the global mapping will not be invertible at all points. This leads us to consider only forward iterates of  $\mathcal{M}$  in the global space.  $\mathcal{M}$  then must be iterated on  $\bigcup_a \partial B_a$ .

In fact, **Condition 2** implies that any outgoing wall  $W \subset \partial B_b^{\text{out}}$ , for some  $b$ , is part of  $\partial B_a^{\text{in}}$ , for  $B_a$  adjacent to  $B_b$  as wall  $W$ , unless  $W$  is only a wall for  $B_b$ , when it lies on the boundary of the whole domain  $\mathcal{U}$ . But **Condition 1** implies that in this case  $W \subset \partial B_b^{\text{in}}$ . Thus,

$$(2.9) \quad \bigcup_{a \in \mathcal{A}} \partial B_a = \bigcup_{a \in \mathcal{A}} \partial B_a^{\text{in}}.$$

So any point on  $\bigcup_{a \in \mathcal{A}} \partial B_a$  belongs to  $\partial B_b^{\text{in}}$  for some  $b \in \mathcal{A}$ . If  $\partial B_a^{\text{out}} \neq \emptyset$ , then  $\mathcal{M}_a$  is well defined by Equation (2.6), but  $\partial B_a^{\text{out}} = \emptyset$  occurs when  $f(a)$  is in the interior of  $B_a$ . In this case,  $f(a)$  is an asymptotically stable steady state, and all points in  $\partial B_a$  are in its basin of attraction, so we can define  $\mathcal{M}_a f(a) = f(a)$ . Then  $\{f(a)\}$  has to be added to the domain of  $\mathcal{M}_a$ .

It is now convenient to introduce the subset of terminal subscripts

$$(2.10) \quad \mathcal{T} = \{a \in \mathcal{A} \mid f(a) \in \text{int}(B_a)\} = \{a \in \mathcal{A} \mid \mathbf{d}(f(a)) = a\}$$

and one can then define local transition maps in all boxes as

$$(2.11) \quad \mathcal{M}_a : x \in \text{Dom}(\mathcal{M}_a) \mapsto \begin{cases} f(a) + ((x_a(0) - f(a))e^{-\Lambda\tau(x_a(0))}) & \text{if } a \in \mathcal{A} \setminus \mathcal{T} \\ f(a) & \text{if } a \in \mathcal{T} \end{cases}$$

It then follows that the domain  $\text{Dom}(\mathcal{M}_a) = \partial B_a^{\text{in}}$  for  $a \in \mathcal{A} \setminus \mathcal{T}$  and  $\text{Dom}(\mathcal{M}_a) = \partial B_a^{\text{in}} \cup \{f(a)\}$  for  $a \in \mathcal{T}$ , and globally,

$$\bigcup_{a \in \mathcal{A}} \text{Dom}(\mathcal{M}_a) = \bigcup_{a \in \mathcal{A}} \partial B_a \cup \bigcup_{a \in \mathcal{T}} \{f(a)\}.$$

A global mapping may still not properly be defined by the above on all of  $\bigcup_{a \in \mathcal{A}} \text{Dom}(\mathcal{M}_a)$ . The problem arises where a  $x \in \text{Dom}(\mathcal{M}_a)$  maps to the intersection of two or more walls, in which case the choice of local map is not unique, and in some cases the subsequent flow depends on this choice. To avoid this issue, following Farcot [11], we exclude all codimension 2 faces from the analysis, along with all points from which those faces can be reached. On such a domain, a global map can be well defined. Farcot expresses the global map in terms of all the local maps for each box  $B_a$  using the indicator function ( $\mathbf{1}_C(x) = 1$  for  $x \in C$ , 0 otherwise) as,

$$(2.12) \quad \mathcal{M}x = \sum_{a \in \mathcal{A}} \mathbf{1}_{\text{Dom}(\mathcal{M}_a)}(x) \mathcal{M}_a x,$$

but defines its domain as

$$(2.13) \quad \mathcal{D} = \bigcup_{a \in \mathcal{A}} \text{Dom}(\mathcal{M}_a) \setminus \bigcup_{k \in \mathbb{N}} \mathcal{M}^{-k}(\mathcal{F}_2),$$

where  $\mathcal{F}_2$  is the union of all threshold faces of codimension 2 or more,  $\mathcal{M}^k$  is the  $k$ th iterate of  $\mathcal{M}$  and  $\mathcal{M}^{-k}(\mathcal{F}_2)$  is the pre-image of the set  $\mathcal{F}_2$ .

Now, as Farcot [11] points out,  $(\mathcal{D}, \mathcal{M})$  is a properly defined one-sided discrete dynamical system, whose orbits are  $\{\mathcal{M}^k x\}_{k \in \mathbb{N}}$ , for  $x \in \mathcal{D}$ . The iterates of  $\mathcal{M}$  are compositions of local maps, as determined by the sequence of walls crossed. The general form of these map compositions are derived by Farcot, but for the purposes of analysis of our later examples, we can restrict ourselves to the case of equal decay

terms:  $\lambda_i = \lambda$ , for all  $i$  and a single threshold for each variable. This implies that  $p_i = 2$  for all  $i$  in Equation (2.3), and all thresholds may be translated to 0, by  $y_i = x_i - \theta_i$  for each  $i$ .

In this case, the analysis follows that of Edwards [6], and the local maps are all piecewise linear:

$$(2.14) \quad \mathcal{M}_a(y) = \frac{B_a y}{1 + \psi_a^\top y},$$

where

$$(2.15) \quad B_a = I - \frac{f(a)\mathbf{e}_j^\top}{f(a)^\top \mathbf{e}_j}, \quad \psi_a = \frac{-\mathbf{e}_j}{f(a)^\top \mathbf{e}_j},$$

and  $\mathbf{e}_j$  is the  $j^{\text{th}}$  standard basis vector, and  $j$  is the index of the exit wall of  $\mathcal{M}_a$ , starting from  $x$ . Note that here,  $B_a$  is not referring to a box as in (2.2), but instead, a mapping.

Then compositions of these fractional linear maps are also fractional linear, and denoting  $\mathcal{M}_{a_k}, B_{a_k}$ , and  $\psi_{a_k}$  more simply as  $\mathcal{M}^{(k)}, B^{(k)}$ , and  $\psi^{(k)}$ , after  $m$  steps the composite map is

$$(2.16) \quad \mathcal{M}^{(m-1)} \dots \mathcal{M}^{(0)} y = \frac{B^{(m,0)} y}{1 + \psi^{(m,0)\top} y},$$

where

$$B^{(m,0)} = B^{(m-1)} \dots B^{(1)} B^{(0)}, \quad \text{and} \quad \psi^{(m,0)} = \psi^{(0)} + \sum_{k=1}^{m-1} B^{(k,0)\top} \psi^{(k)}.$$

Thus, for a cycle, where after  $m$  steps the trajectory returns to its initial wall (we may say  $W^{(m)} = W^{(0)}$ , using the same numbering for walls as for the maps), we have

$$(2.17) \quad \mathcal{M} : W^{(0)} \rightarrow W^{(0)}, \quad \mathcal{M} y = \frac{B y}{1 + \psi^\top y},$$

with  $B = B^{(m,0)}$  and  $\psi = \psi^{(m,0)}$ .

**3. Symbolic Dynamics Approach.** As discussed in the previous section, the dynamics of Glass networks can be represented (without loss of information) using a continuous-space, discrete-time dynamical system. This discretization process can be taken a step further to discretize space as well. Glass network dynamics can be qualitatively represented using symbolic dynamical systems and as a result, techniques from symbolic dynamics can be used to draw useful conclusions about the original system. The following is a summary of the construction used by Farcot to analyze the irregularity of Glass network dynamics using symbolic dynamics. For a detailed description of the construction, see Farcot [11].

The partitioning of phase space into boxes along with the transition maps between them allows a natural encoding of the allowable dynamics of the system in terms of a directed graph, called a transition graph and denoted  $\text{TG} = (\mathcal{A}, \mathcal{E})$ . The TG vertices are box subscripts and the edges correspond to pairs of boxes that can be successively crossed by a trajectory. This includes 1-loops, to handle the case of a focal point in the interior of its own box,  $f(a) \in \text{int}(B_a)$ , and pairs that are adjacent through an  $(n-1)$ -dimensional wall. By **Condition 2**,  $B_a$  and  $B_b$  are adjacent via a single wall if and



only if  $a - b = \pm \mathbf{e}_i$ , for  $i \in \{1, \dots, n\}$ . Trajectories traversing a box  $B_a$  can only exit through a wall  $W_i^\pm$  for  $i \in I_{\text{out}}(a)$  with the direction given by  $\pm_i = \text{sign}(\mathbf{d}_i(f(a)) - a_i)$ . Thus, the edge set of the TG is

$$\mathcal{E} = \{(a, a) \mid a \in \mathcal{T}\} \cup \{(a, a \pm_i \mathbf{e}_i) \mid a \in \mathcal{A} \setminus \mathcal{T}, i \in I_{\text{out}}(a)\}.$$

The TG describes transitions between boxes that can occur through faces that have dimension  $(n - 1)$ , *i.e.*, through interiors of walls. Now, attractors of the continuous-space, discrete time system  $(\mathcal{D}, \mathcal{M})$  have a counterpart in the TG, but the converse does not hold in general since trajectories on the TG may correspond to no trajectories in the original continuous-space system. Some information has been lost in going to the TG dynamics. We will take this point up again in the next Section.

The TG encodes the possible dynamics of  $(\mathcal{D}, \mathcal{M})$  into a subset of infinite words on the alphabet  $\mathcal{A}$ . The words are given by infinite paths on the graph and the set of all words is given by

$$\mathcal{J}(\text{TG}) = \{\mathbf{a} = (a^t)_{t \in \mathbb{N}} \mid \forall t \in \mathbb{N}, (a^t, a^{t+1}) \in \mathcal{E}\} \subset \mathcal{A}^{\mathbb{N}}.$$

$\mathcal{J}(\text{TG})$  can be endowed with a metric to make it a metric space, on which discrete dynamics can be defined by the shift operator  $\sigma : \mathcal{J}(\text{TG}) \rightarrow \mathcal{J}(\text{TG})$ , where  $(\sigma(\mathbf{a}))^t = a^{t+1}$ . This operator is continuous, for example, in the metric

$$(3.1) \quad \rho(\mathbf{a}, \mathbf{b}) = \begin{cases} 0 & \text{if } \mathbf{a} = \mathbf{b}, \\ 2^{-\min\{t \mid a^t \neq b^t\}} & \text{if } \mathbf{a} \neq \mathbf{b}. \end{cases}$$

The more initial terms of  $\mathbf{a}$  and  $\mathbf{b}$  coincide, the smaller the distance between them, according to this metric. Additionally,  $\mathcal{J}(\text{TG})$  is compact for the metric  $\rho$  and is  $\sigma$ -invariant. As a result,  $\mathcal{J}(\text{TG})$  is a shift space, where  $(\mathcal{J}(\text{TG}), \sigma)$  constitutes a discrete dynamical system. Since orbits of this system are associated with words defined on the alphabet  $\mathcal{A}$ , whose elements in turn represent subsets of the state space of the initial dynamical system, the trajectories of  $(\mathcal{J}(\text{TG}), \sigma)$  represent sets of trajectories in  $(\mathcal{D}, \mathcal{M})$ .

These two dynamical systems can be compared by means of a mapping  $\phi : \mathcal{D} \rightarrow \mathcal{J}(\text{TG})$ , which could lead to the conjugation relation  $\phi \circ \mathcal{M} = \sigma \circ \phi$ . If  $\phi$  is a homeomorphism it is then called a topological conjugacy. Topologically, two conjugate dynamical systems behave identically. Now,  $\mathcal{D}$  lies in the union of all faces of boxes taken without their boundary. Any of these open faces is well defined by the two boxes it is a part of, except those on the boundary  $\partial\mathcal{U}$ , but since this boundary cannot be reached from the rest of  $\mathcal{D}$ , we can ignore it and redefine  $\mathcal{D}$  as  $\mathcal{D} \setminus \partial\mathcal{U}$ . So now  $\forall x \in \mathcal{D}$ , there is either a unique pair  $(a, b)$  such that  $x \in \partial B_a^{\text{out}} \cap \partial B_b^{\text{in}}$ , or some  $a \in \mathcal{T}$  such that  $x \in \partial B_a \cup \{f(a)\}$ . We can now define a map  $\Phi : \mathcal{D} \rightarrow \mathcal{E}$  as

$$(3.2) \quad \Phi(x) = \begin{cases} (a, b) & \text{if } x \in \partial B_a^{\text{out}} \cap \partial B_b^{\text{in}} \\ (a, a) & \text{if } x \in \partial B_a \cup \{f(a)\}, \text{ for } a \in \mathcal{T} \end{cases}$$

so that  $\Phi$  maps to edges of the TG instead of vertices. Note that  $\Phi^{-1}(a, b)$  is the open wall between two adjacent boxes  $B_a$  and  $B_b$ . This then leads us to consider a new shift space obtained from  $\mathcal{J}(\text{TG})$  through the 2-block map  $\beta_2$  defined as

$$(\beta_2(\mathbf{a}))^t = \begin{bmatrix} a^t \\ a^{t+1} \end{bmatrix} \in \mathcal{E}$$

where  $\mathcal{J}(\text{TG})^{[2]} = \beta_2(\mathcal{J}(\text{TG})) \subset \mathcal{E}^{\mathbb{N}}$  is a shift space. The shift operator on  $\mathcal{J}(\text{TG})^{[2]}$  is then denoted as  $\sigma_{[2]}$ . Since  $\beta_2$  is continuous and  $\beta_2 \circ \sigma = \sigma_{[2]} \circ \beta_2$ ,  $(\mathcal{J}(\text{TG}), \sigma)$  and  $(\mathcal{J}(\text{TG})^{[2]}, \sigma_{[2]})$  are conjugate dynamical systems.

Now to encode the trajectories from  $(\mathcal{D}, \mathcal{M})$  there are two steps. First, define the mapping  $\xi : \mathcal{D} \rightarrow \mathcal{D}^{\mathbb{N}}$  by  $\xi(x) = (x, \mathcal{M}x, \mathcal{M}^2x, \dots)$ . Since  $\mathcal{M}$  is continuous on  $\mathcal{D}$  it can be proven that  $\xi$  is a conjugacy when its range is restricted to  $\xi(\mathcal{D})$  (see Farcot [11] for details). The second is the mapping  $\Phi_{\infty} : \mathcal{D}^{\mathbb{N}} \rightarrow \mathcal{J}(\text{TG})^{[2]}$ , given by

$$\Phi_{\infty}((x^k)_{k \in \mathbb{N}}) = (\Phi(x^k))_{k \in \mathbb{N}}.$$

Here  $\Phi_{\infty}$  maps sequences in  $\mathcal{D}$  to sequences in  $\mathcal{E}$ . Finally, the map  $\phi$  is defined as

$$\phi = \Phi_{\infty} \circ \xi : \mathcal{D} \rightarrow \mathcal{J}(\text{TG})^{[2]}$$

It is shown by Farcot [11] that the mapping  $\phi$  takes constant values on the domains

$$D_a = \bigcap_{j \in \mathbb{N}} \mathcal{M}^{-j}(\Phi^{-1}(a^j, a^{j+1}))$$

which are exactly the connected components of  $\mathcal{D}$ . Hence,  $\phi$  is continuous.

Now it is clear that  $\Phi_{\infty}$ , and thus  $\phi$ , is neither injective nor surjective in general. The non-injectivity of  $\phi$  is an inevitable feature of the system  $(\mathcal{D}, \mathcal{M})$ , in which the domains  $D_a$  associated with admissible itineraries are not single points. The fact that  $\phi$  is not surjective means that some infinite paths on the transition graph do not correspond to any admissible trajectory of the continuous-space system. The TG represents transitions between boxes that are individually feasible, but there is no guarantee that a finite sequence of such transitions is feasible. Thus,  $\phi(\mathcal{D}) \subset \mathcal{J}(\text{TG})^{[2]}$  is a proper subset, and exactly the space of admissible trajectories in TG. As detailed by Farcot [11],  $\phi(\mathcal{D})$  inherits shift-invariance from  $\mathcal{D}$ 's  $\mathcal{M}$ -invariance. Now, the space  $\phi(\mathcal{D})$  must be compact in order for it to be a properly defined symbolic dynamical system. Since  $\mathcal{J}(\text{TG})^{[2]}$  is compact and contains  $\phi(\mathcal{D})$  it would suffice to show that  $\phi(\mathcal{D})$  is closed. However, it turns out that  $\phi(\mathcal{D})$  is not closed in general.

Now there are two equivalent characterizations of shift spaces: they can be defined as shift-invariant compact subspaces of the full shift, or as subspaces of all infinite words on the alphabet defined by a set of forbidden blocks. Now since  $\phi$  is constant on each  $D_a$ ,  $\phi(\mathcal{D})$  is the set of words  $\epsilon = \beta_2(a)$  such that  $D_a \neq \emptyset$ . Letting  $D_a^i = \bigcap_{k=0}^i \mathcal{M}^{-k}(\Phi^{-1}(a^k, a^{k+1}))$ , where  $D_a = \bigcap_{i \in \mathbb{N}} D_a^i$  is empty if either one  $D_a^i$  is empty or all of them are nonempty but their full intersection is. In the latter case  $\beta_2(a)$  is an infinite word that is forbidden in  $\phi(\mathcal{D})$  while all its subwords are allowed. Thus, it does not satisfy the first characterization of a shift space. Naturally then the system to consider is  $(\overline{\phi(\mathcal{D})}, \sigma_{[2]})$ . This one is a properly defined symbolic dynamical system since the closure  $\overline{\phi(\mathcal{D})}$  is clearly compact. Now, the dynamics of the two symbolic dynamical systems  $(\overline{\phi(\mathcal{D})}, \sigma_{[2]})$  and  $(\mathcal{J}(\text{TG})^{[2]}, \sigma_{[2]})$  may be compared. In order to compare the dynamics of the systems  $(\overline{\phi(\mathcal{D})}, \sigma_{[2]})$  and  $(\mathcal{J}(\text{TG})^{[2]}, \sigma_{[2]})$ , we will now consider the quantity topological entropy. In dynamical systems, topological entropy is a nonnegative number that is a measure of the complexity of the dynamical system. Nonzero values of topological entropy are often taken as an indicator of dynamical chaos.

In symbolic dynamics, topological entropy is conjugacy invariant and can be computed easily for systems described by directed graphs. This makes it a useful tool

for comparing symbolic dynamical systems. We first give the classical definition of topological entropy for symbolic dynamical systems. Let  $X$  be a shift space. The topological entropy of  $X$  is defined by

$$(3.3) \quad h(X) = \lim_{n \rightarrow \infty} \frac{1}{n} \log |\mathcal{B}_n(X)|$$

where  $|\mathcal{B}_n(X)|$  is the number of blocks of length  $n$  for the shift space  $X$ , and  $\log$  is by convention the logarithm with base 2. By definition  $h(X)$  is nonnegative; for chaotic dynamical systems this value is positive. In the case when  $X$  is defined by the way of infinite paths on an oriented graph  $G$ , let  $A$  be the adjacency matrix of  $G$ :  $A_{i,j} \in \{0, 1\}$ , and  $A_{i,j} = 1$  if and only if  $(i, j)$  is an edge in the graph. Define the irreducible components of  $A$  as the equivalence classes for the equivalence relation:  $i \sim j$  if  $\exists p, q \in \mathbb{N}, (A^p)_{i,j} \neq 0$  and  $(A^q)_{j,i} \neq 0$ . This corresponds exactly to the strongly connected components in  $G$ . Let  $A_i, i = 1, \dots, k$  be the sub-matrices of  $A$  with all indices in the same equivalence class. If there is a single class,  $A$  is said to be irreducible. The Perron-Frobenius theorem ensures that any irreducible matrix with nonnegative entries has a dominant positive eigenvalue  $\mu_A$ , which is simple, and is associated with a nonnegative eigenvector. Following Lind and Marcus [28], the Perron eigenvalue of  $A$  is  $\mu_A = \max_{i=1, \dots, k} \mu_{A_i}$  where each  $\mu_{A_i}$  is the Perron eigenvalue of each irreducible sub-matrix,  $A_i$ , and the entropy is given by

$$(3.4) \quad h(X) = \log \mu_A.$$

Finally, since  $\mathcal{J}(\text{TG})$  and  $\mathcal{J}(\text{TG})^{[2]}$  are conjugate and topological entropy is conjugacy invariant it follows that they have the same topological entropy. As  $\mathcal{J}(\text{TG})$  is exactly the shift space induced by infinite paths on the TG, one simply defines

$$h_{\text{TG}} = h(\mathcal{J}(\text{TG})^{[2]}) = h(\mathcal{J}(\text{TG})).$$

One can then also define the entropy of the true dynamics as  $h_{\phi(\mathcal{D})} = h(\overline{\phi(\mathcal{D})})$ . Finally, since we have that  $\overline{\phi(\mathcal{D})} \subset \mathcal{J}(\text{TG})^{[2]}$ , it follows that  $h_{\phi(\mathcal{D})} \leq h_{\text{TG}}$ .

**4. An Improved Upper Bound.** In the previous two sections we discussed the construction from [11] that allows for  $(\mathcal{D}, \mathcal{M})$  to be mapped into  $(\overline{\phi(\mathcal{D})}, \sigma_{[2]})$ . The entropy of  $(\overline{\phi(\mathcal{D})}, \sigma_{[2]})$  is then shown to be bounded above by the entropy of the TG, which is an indication of the potential irregularity of the system dynamics. However, for many Glass networks the entire set of dynamics allowed by the TG may not be realized in the continuous dynamics after transients, so this upper bound on entropy may be very loose. When there exists a *trapping region* in phase space, *i.e.*, a positively invariant region from which trajectories cannot escape, then the system dynamics may be constrained to a subset of the TG. It may be that all trajectories are eventually confined to one trapping region, but even if there are other attractors, once confined to a trapping region, the entropy of the subsequent dynamics is unaffected by other parts of phase space. Thus, once transients have died out, the long term dynamics can be represented using the subset of the TG that represents only the trapping region, and the corresponding entropy provides a tighter upper bound than the full TG.

In order to quantify this improved upper bound on entropy a few definitions will be needed, starting with *cycles*.

DEFINITION 4.1. Given a starting wall  $\omega_1$ , a cycle,  $\mathcal{C}$ , through  $\omega_1$  is defined as a sequence of boxes  $(a_i)_{i=1}^n$  through walls  $(\omega_i)_{i=1}^{n+1}$  (where  $\omega_{n+1} = \omega_1$ ), consistent with the flow such that  $\omega_i$  is the entry wall to box  $a_i$ , and the length of the cycle is  $n$ .

In general, many trajectories follow a given cycle, at least once, from a starting wall back to the same wall. Since boxes can have multiple exit walls, each wall along the cycle can be partitioned into regions corresponding to each possible subsequent exit wall, as described in Section 2. The region on a wall that maps through a particular sequence of subsequent walls will in general be an even smaller region, since not all of the region on the first wall that maps to the second may then map to the third, etc. In order for a trajectory passing through a starting wall to follow a cycle and return back to that wall, the trajectory must be confined to the region in each wall that maps through the rest of the walls in the cycle. To specify the region of phase space occupied by trajectories following the cycle, or at least its intersections with each wall around the cycle, we first define the *returning region* on the starting wall.

DEFINITION 4.2. Let  $\mathcal{C}$  be a cycle of boxes of length  $n$  with starting wall  $\omega_1$ . The returning region of  $\mathcal{C}$  on wall  $\omega_1$  is the subset of  $\omega_1$  that under  $n$  applications of the map  $\mathcal{M}$  will return back to  $\omega_1$ . Letting  $RC_i(S) = \mathcal{M}^{-1}(S) \cap \omega_i$ , this subset is defined as

$$(4.1) \quad \mathcal{RC}_{\mathcal{C}}(\omega_1) = RC_1 \circ \dots \circ RC_n(\omega_1).$$

The cycle map,  $\mathcal{M}_{\mathcal{C}} : \mathcal{RC}_{\mathcal{C}}(\omega_1) \rightarrow \omega_1$  is defined by  $\mathcal{M}_{\mathcal{C}}(x) = \mathcal{M}^n(x)$ .

When all decay rates in the Glass network are equal (but not in general), these returning regions are polygonal cones, hence the notation  $\mathcal{RC}$ , for *returning cone*.

The subset of  $\mathcal{D}$  through which trajectories starting in this returning region  $\mathcal{RC}_{\mathcal{C}}(\omega_1)$  pass is now defined as follows.

DEFINITION 4.3. For a cycle  $\mathcal{C}$  of length  $n$  with starting wall  $\omega_1$ , the subset of the domain  $\mathcal{D}$  traversed by trajectories following cycle  $\mathcal{C}$  is

$$(4.2) \quad \mathcal{D}_{\mathcal{C}} = \mathcal{D} \cap \bigcup_{i=0}^{n-1} \mathcal{M}^i(\mathcal{RC}_{\mathcal{C}}(\omega_1))$$

where  $\mathcal{M}^0 = id$ . We call this the *cycle tube* associated with cycle  $\mathcal{C}$ .

Using these definitions we can now define a trapping region for a Glass network.

DEFINITION 4.4. For a given Glass network, and a given starting wall,  $\omega_1$ , a trapping region in wall  $\omega_1$  consisting of  $N_c$  cycles is defined as

$$(4.3) \quad \bigcup_{i=1}^{N_c} \mathcal{RC}_{\mathcal{C}_i}(\omega_1),$$

where

$$\bigcup_{i=1}^{N_c} \mathcal{M}_{\mathcal{C}_i}(\mathcal{RC}_{\mathcal{C}_i}(\omega_1)) \subseteq \bigcup_{i=1}^{N_c} \mathcal{RC}_{\mathcal{C}_i}(\omega_1),$$

and its corresponding trapping tube is defined as

$$(4.4) \quad \mathcal{D}_{TR} = \bigcup_{i=1}^{N_c} \mathcal{D}_{\mathcal{C}_i}.$$

We note here that transients can often be removed to obtain a smaller trapping region before proceeding with the analysis. In the context of our trapping region and trapping tube, a transient region is any returning region that is non-empty, but after an initial cycle back to the starting wall, is never visited again. This is the case when there are nonempty returning regions that nothing maps into. If the returning region of a transient cycle is removed from the trapping region, one is left with a smaller trapping region. Transient regions can be defined as follows.

**DEFINITION 4.5.** *For a given Glass network with a trapping region as defined above, if there exists a cycle  $\mathcal{C}_j$  with  $1 \leq j \leq N_c$ , (one of the cycles that forms the trapping region), such that*

$$\bigcup_{i=1}^{N_c} \mathcal{M}_{\mathcal{C}_i}(\mathcal{R}\mathcal{C}_{\mathcal{C}_i}(\omega_1)) \cap \mathcal{R}\mathcal{C}_{\mathcal{C}_j}(\omega_1) = \emptyset,$$

*then  $\mathcal{C}_j$  is a transient cycle (sequence of box transitions) and its returning region is a transient region on the wall  $\omega_1$ .*

We can obtain a trapping region with transients removed for a given Glass network and a given starting wall,  $\omega_1$ , as follows. If the trapping region consisting of  $N_c$  cycles is as given by (4.3), and there exist transient cycles  $\mathcal{C}_{i_k}$  with  $0 \leq i_k \leq N_c$ , for each  $k = 1, \dots, N_T$ , then the smaller trapping region is

$$(4.5) \quad \bigcup_{i=1}^{N_c} \mathcal{R}\mathcal{C}_{\mathcal{C}_i}(\omega_1) \setminus \bigcup_{k=1}^{N_T} \mathcal{R}\mathcal{C}_{\mathcal{C}_{i_k}}(\omega_1),$$

since

$$\bigcup_{i=1}^{N_c} \mathcal{M}_{\mathcal{C}_i}(\mathcal{R}\mathcal{C}_{\mathcal{C}_i}(\omega_1)) \subseteq \bigcup_{i=1}^{N_c} \mathcal{R}\mathcal{C}_{\mathcal{C}_i}(\omega_1) \setminus \bigcup_{k=1}^{N_T} \mathcal{R}\mathcal{C}_{\mathcal{C}_{i_k}}(\omega_1),$$

or relabelling the remaining  $N_{c'} = N_c - N_T$  cycles as  $\mathcal{C}'_j, 1 \leq j \leq N_{c'}$ , the smaller trapping region is

$$(4.6) \quad \bigcup_{j=1}^{N_{c'}} \mathcal{R}\mathcal{C}_{\mathcal{C}'_j}(\omega_1),$$

and its trapping tube is

$$(4.7) \quad \mathcal{D}_{TR} = \bigcup_{i=1}^{N_c} \mathcal{D}_{\mathcal{C}_i} \setminus \bigcup_{k=1}^{N_T} \mathcal{D}_{\mathcal{C}_{i_k}} = \bigcup_{i=1}^{N_{c'}} \mathcal{D}_{\mathcal{C}'_i}.$$

Similarly, one could also define as transients regions  $\mathcal{C}_j$  such that the image after a finite number of iterations of the set of cycle maps (rather than just 1 iteration) does not intersect with  $\mathcal{R}\mathcal{C}_{\mathcal{C}_j}(\omega_1)$ . However, the notation becomes more cumbersome.

We are interested in Glass networks in which such a trapping region occurs. To ensure that we are considering only relevant systems we now impose a third condition on the network:

**Condition 3.** There exists a wall that is returned to infinitely often via a finite number of cycles. The returning regions of these cycles partition the wall or a subset of the wall into a finite number of regions such that their union is a trapping region.

This condition avoids the situation where there are an infinite number of cycles whose returning regions form an infinite partition of the wall. Later in our analysis, an infinite number of cycles will lead to infinite alphabets in the derived symbolic dynamical systems, and we prefer not to deal with such difficulties. In most of the examples we have looked at, this situation does not arise, but an example of such a system was presented by Gedeon [15].

This condition also means that there is a starting wall (or a subset) to which trajectories always return, and which is therefore itself a trapping region, with a corresponding graph that is, potentially, a proper subset of the TG.

We will further assume that we have a minimal trapping region, in the sense that it is not the union of disjoint sets that are themselves trapping regions. Multiple trapping regions correspond to different attractors, each with their own entropy, and we focus here on the entropy of a single attractor.

In order to represent dynamics, we can define the trapping region graph by  $\text{TG}_r = (\mathcal{A}_r, \mathcal{E}_r)$  where  $\mathcal{A}_r = \bigcup_{i=1}^{N_c} \mathcal{C}_i \subseteq \mathcal{A}$ ,

$$\mathcal{E}_r = \bigcup_{j=1}^{N_c} \{(a_{i,j}, a_{i+1,j}) | a_{i,j} \in \mathcal{C}_j\}$$

and  $\mathcal{C}_j = (a_{i,j})_{i=1}^{n_j}$ , which is of length  $n_j$  and we identify  $a_{n_j+1,j}$  with  $a_{1,j}$ .

As in the previous section,  $\text{TG}_r$  encodes the possible dynamics of  $(\mathcal{D}_{\text{TR}}, \mathcal{M})$  into a subset of infinite words on the alphabet  $\mathcal{A}_r$ . The words are similarly given by infinite paths on  $\text{TG}_r$  and the set of all words is given by

$$\mathcal{J}(\text{TG}_r) = \{\mathbf{a} = (a^t)_{t \in \mathbb{N}} | \forall t \in \mathbb{N}, (a^t, a^{t+1}) \in \mathcal{E}_r\} \subset \mathcal{A}^{\mathbb{N}}.$$

It should be clear from this definition that  $\mathcal{E}_r \subseteq \mathcal{E}$  and  $\mathcal{J}(\text{TG}_r) \subseteq \mathcal{J}(\text{TG})$ . In order to compare the continuous dynamics to the dynamics of  $\mathcal{J}(\text{TG}_r)$  we must apply the 2-block map to obtain  $\mathcal{J}(\text{TG}_r)^{[2]} = \beta_2(\mathcal{J}(\text{TG}_r)) \subseteq \mathcal{E}_r^{\mathbb{N}} \subseteq \mathcal{E}^{\mathbb{N}}$ . It follows that  $\mathcal{J}(\text{TG}_r)^{[2]} \subseteq \mathcal{J}(\text{TG})^{[2]}$ . Now we must encode the trajectories of  $(\mathcal{D}_{\text{TR}}, \mathcal{M})$  in order to compare the dynamics on the trapping region to  $\mathcal{J}(\text{TG}_r)^{[2]}$ . The space of admissible trajectories in  $\text{TG}_r$  is then exactly  $\phi(\mathcal{D}_{\text{TR}})$ . We encounter the same problem with  $\mathcal{D}_{\text{TR}}$  as we did with  $\mathcal{D}$ , namely, that  $\phi(\mathcal{D}_{\text{TR}})$  is not compact. So in order to properly define a symbolic dynamical system we must consider the closure,  $\overline{\phi(\mathcal{D}_{\text{TR}})}$ . It follows that  $\overline{\phi(\mathcal{D}_{\text{TR}})} \subseteq \mathcal{J}(\text{TG}_r)^{[2]} \subseteq \mathcal{J}(\text{TG})^{[2]}$ . Finally, defining the entropies  $h_{\phi(\mathcal{D}_{\text{TR}})} = h(\overline{\phi(\mathcal{D}_{\text{TR}})})$  and  $h_{\text{TG}_r} = h(\mathcal{J}(\text{TG}_r)^{[2]}) = h(\mathcal{J}(\text{TG}_r))$  it follows that  $h_{\phi(\mathcal{D}_{\text{TR}})} \leq h_{\text{TG}_r} \leq h_{\text{TG}}$ . Thus, the entropy of the  $\text{TG}_r$  is potentially a better upper bound on the entropy of the true dynamics than is the original TG.

**5. An Example.** To demonstrate the efficacy of reducing the TG to the  $\text{TG}_r$ , *i.e.*, the reduction of the upper bound on entropy, we now introduce an illustrative example, which we will continue to use to illustrate further improvements in the next section. Consider the following Glass network:

$$\begin{aligned} \dot{y}_1 &= -y_1 + 2(\bar{Y}_3 Y_4 + Y_2 Y_3) - 1 \\ \dot{y}_2 &= -y_2 + 2(Y_1 \bar{Y}_3 Y_4 + \bar{Y}_1 Y_3 Y_4 + \bar{Y}_1 \bar{Y}_3 \bar{Y}_4) - 1 \\ \dot{y}_3 &= -y_3 + 2(\bar{Y}_1 Y_2 + Y_1 Y_4) - 1 \\ \dot{y}_4 &= -y_4 + 2(Y_2 \bar{Y}_3 + \bar{Y}_1 Y_3) - 1 \end{aligned} \tag{5.1}$$

where  $Y_i = 0$  if  $y_i < 0$ , and 1 if  $y_i > 0$ .  $\bar{Y}_i = 1 - Y_i$ . This network is simple in the sense that all its degradation rates are 1, all the focal points are located at  $\pm 1$ , and each

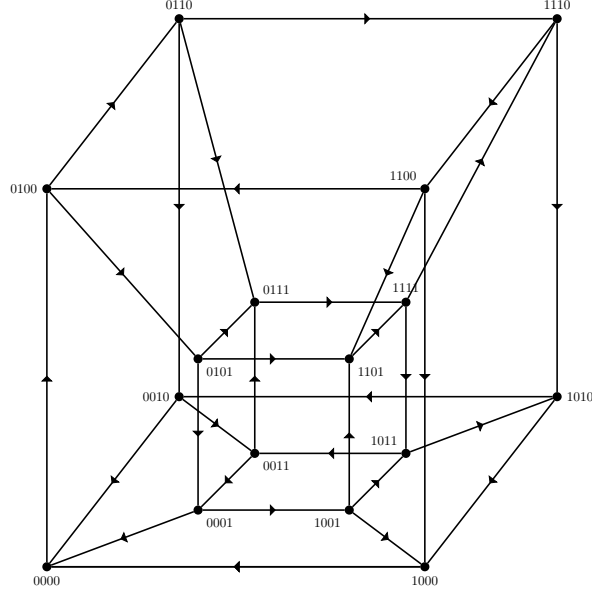


Fig. 5.1: TG for example Glass network.

variable has only a single threshold. Its TG can be represented by the 4-dimensional hypercube in Figure 5.1 (see [7]). From the adjacency matrix of the TG, we calculate the entropy (the logarithm of the Perron eigenvalue) to be  $h_{\text{TG}} \approx 0.873$ .

Now, using the wall between boxes 1111 and 1110 as a starting wall (which we may denote  $++ +0$  to indicate the sign of each  $y_i$ ), among the many cycles on the TG that return to this wall are two, denoted  $A$  and  $B$ , that form a trapping region [7].

$$A : 1110 \rightarrow 1010 \rightarrow 0010 \rightarrow 0000 \rightarrow 0100 \rightarrow 0110 \rightarrow 0111 \rightarrow 1111,$$

$$B : 1110 \rightarrow 1010 \rightarrow 0010 \rightarrow 0011 \rightarrow 0001 \rightarrow 0000 \rightarrow 0100 \rightarrow 0101 \rightarrow 0111 \rightarrow 1111.$$

To show that the returning cones for these two cycles form a trapping region, one calculates the returning cones for each cycle and shows that their images under their respective cycle maps lie in the union of their returning cones. Thus, any trajectory that follows cycle  $A$  or  $B$  once will necessarily follow one or the other at each iteration for the rest of time. Projections of example trajectories are shown in Figure 5.2.

As detailed in Section 4, one way of computing a cycle's returning cone is to map the starting wall backwards through the cycle using the inverse map  $\mathcal{M}^{-1}$  and intersect these images with each wall along the cycle. In practice, this means identifying which region on a wall maps to the correct region in the next wall. Outside this region, a different wall (not the one following the cycle) will be reached at the next or a subsequent step. Thus, whenever an entry wall to a box along the cycle maps to multiple exit walls, an inequality must be satisfied on the entry wall for each alternative exit variable to ensure that such a diversion from the cycle does not occur. These inequalities must then be mapped back from the relevant entry wall to the starting wall. The inequality to prevent an alternative exit on the  $k^{\text{th}}$  wall of the cycle is [7]

$$(5.2) \quad -\frac{\mathbf{e}'_i}{f_i^{(k)}} B^{(k)} \mathbf{y}^{(k)} > 0, ,$$

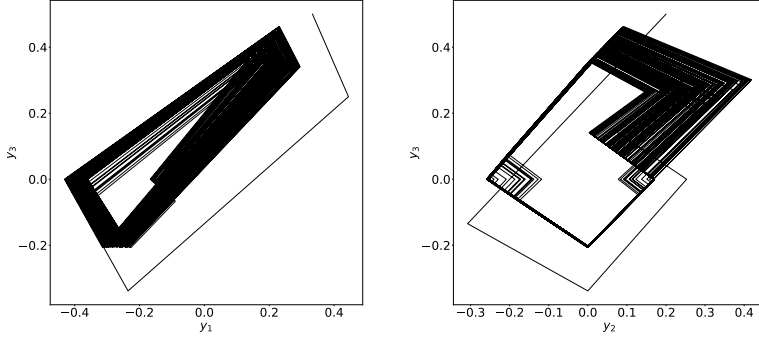


Fig. 5.2: Phase portraits for example Glass network

where  $i$  represents an alternative exit direction, and the denominator of the map (2.14), which is necessarily positive, has been omitted. Note that there may be more than one such  $i$  for a given wall.

The corresponding inequality on the starting wall is

$$(5.3) \quad -\frac{\mathbf{e}'_i}{f_i^{(k)}} B^{(k)} B^{(k-1)} \dots B^{(0)} \mathbf{y}^{(0)} > 0.$$

The region satisfying this inequality on the starting wall gets mapped to the region on the  $k^{\text{th}}$  wall that satisfies the inequality (5.2). Thus, in order for a trajectory starting on the starting wall to return to the starting wall following the given cycle, it must satisfy the set of inequalities (5.3) for each alternative exit variable around the cycle. This set of inequalities defines the returning cone:

$$(5.4) \quad C = \{\mathbf{y} \in \omega_1 \mid R\mathbf{y} \geq 0\}$$

where  $\omega_1$  is the starting boundary and  $R$  is a matrix with one row for each alternate exit variable around the cycle, given by

$$(5.5) \quad R_i = -\frac{\mathbf{e}'_i}{f_i^{(k)}} B^{(k)} B^{(k-1)} \dots B^{(0)}$$

as in the left hand side of (5.3).

For cycle  $A$  in our example network, from the starting wall there is one alternative exit variable,  $i = 3$ . On the next wall,  $+0+-$  (between boxes 1110 and 1010),  $i = 3$  is again the only alternative exit variable. On the next wall,  $0-+-$  (between boxes 1010 and 0010) the only alternative exit variable is  $i = 4$ . Then, on  $--0-$  (between boxes 0010 and 0000), there are no alternative exit variables so this wall does not contribute a row to the matrix  $R$ . On the wall  $-0--$  (between boxes 0000 and 0100), there is one alternative exit variable,  $i = 4$ . On  $-+0-$  (between boxes 0100 and 0110), there are two alternative exit variables,  $i = 1$  and  $i = 2$ . On  $-++0$  (between boxes 0110 and 0111), there are no alternative exit variables. Finally, on the last wall of the cycle,  $0+++$  (between boxes 0111 and 1111), there is one alternative exit variable,  $i = 2$ .



Using all of these alternative exit variables for cycle  $A$  in equation (5.5), we compute the matrix  $R$  for cycle  $A$  as

$$R_A = \begin{pmatrix} 0 & -1 & 1 & 0 \\ -1 & -2 & 1 & 0 \\ 2 & 4 & -1 & -1 \\ 2 & 4 & -1 & -1 \\ -3 & -8 & 4 & 1 \\ -2 & -5 & 2 & 1 \\ -2 & -5 & 2 & 1 \end{pmatrix}.$$

Because necessarily  $y_4 = 0$  on the starting wall, we can ignore the final column of  $R_A$ , and by a slight abuse of notation let  $\mathbf{y}$  denote just  $(y_1, y_2, y_3)^\top$ . We can also remove duplicate rows of  $R_A$ , and actually we can remove rows for which the inequality is already implied by another row or rows. Removing all such redundancies,  $R_A$  becomes

$$(5.6) \quad R_A = \begin{pmatrix} 2 & 4 & -1 \\ -2 & -5 & 2 \end{pmatrix}.$$

Similarly, following the same procedure, the  $R$  matrix that defines the returning cone for cycle  $B$  is

$$(5.7) \quad R_B = \begin{pmatrix} 6 & 11 & -2 \\ -2 & -4 & 1 \end{pmatrix}.$$

We can also describe the returning cones by means of their extremal vectors (vertices of a polygonal cross section of the cone) [7]. Berman and Plemmons [3] define a cone as follows.

DEFINITION 5.1. *For a set  $S \subseteq \mathbb{R}^n$ , the set generated by  $S$  is the set of finite non-negative linear combinations of elements of  $S$ :*

$$S^G = \left\{ \sum_{i=1}^m c_i x_i, \text{ for some } c_i \geq 0, x_i \in S, m \text{ finite} \right\}.$$

A set  $K$  is a cone if  $K = K^G$ , so for any  $S$ ,  $S^G$  is a cone.

Then the returning cones for cycles  $A$  and  $B$  are (respectively):

$$(5.8) \quad C_A = \left\{ \left(0, \frac{2}{7}, \frac{5}{7}\right)^\top, \left(\frac{1}{2}, 0, \frac{1}{2}\right)^\top, \left(\frac{1}{3}, 0, \frac{2}{3}\right)^\top, \left(0, \frac{1}{5}, \frac{4}{5}\right)^\top \right\}^G,$$

$$(5.9) \quad C_B = \left\{ \left(0, \frac{2}{13}, \frac{11}{13}\right)^\top, \left(\frac{1}{4}, 0, \frac{3}{4}\right)^\top, \left(\frac{1}{3}, 0, \frac{2}{3}\right)^\top, \left(0, \frac{1}{5}, \frac{4}{5}\right)^\top \right\}^G.$$

On  $C_A$  and  $C_B$  their respective cycle maps act together as a Poincaré map. Since the cycle map acts on (a subset of) the starting wall, which is in  $\mathbb{R}^{n-1}$ , we can express it in terms of  $(n-1)$ -vectors and an  $(n-1) \times (n-1)$  matrix. On the starting wall one of the coordinates is always zero ( $y_i = 0$ ), so we can remove it from the cycle map. Also, since in the computation of the cycle matrix the  $i^{\text{th}}$  row is all 0's, we can remove that row also. So we can reduce the cycle map for a given cycle by one row

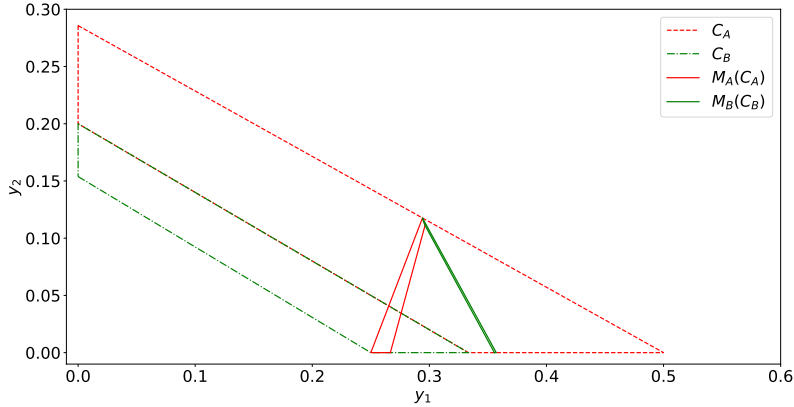


Fig. 5.3: Returning cones for cycles  $A$  and  $B$  in the example, represented by the cross section in the plane  $y_1 + y_2 + y_3 = 1$  with only the first two coordinates plotted, and their images under their respective cycle maps.

and column. For this example we can write the map (2.17) for each of the cycles in terms of  $3 \times 3$  matrices, and 3-vectors as

$$M_A = \frac{A\mathbf{y}}{1 + \phi^\top \mathbf{y}}, \quad M_B = \frac{B\mathbf{y}}{1 + \psi^\top \mathbf{y}},$$

where

$$A = \begin{pmatrix} -3 & -8 & 4 \\ -2 & -5 & 2 \\ -4 & -12 & 7 \end{pmatrix}, \quad B = \begin{pmatrix} 5 & 8 & 0 \\ 6 & 11 & -2 \\ 12 & 20 & -1 \end{pmatrix},$$

$$\phi = (-4, -14, 10)^\top, \quad \psi = (12, 18, 2)^\top.$$

Applying each of the cycle maps to their respective returning cones, one finds that each returning cone gets mapped into the union of the two. Returning cones are proper (non-empty, pointed) cones in  $\mathbb{R}^{n-1}$  (a wall in  $\mathbb{R}^n$ ) with vertex at the origin. In a Glass network with uniform decay rates, rays map to rays under the mappings from wall to wall and radial dynamics is always convergent (trajectories starting on the same ray converge under iteration of the maps) [6]. So, in order to depict where returning cones,  $C_A$  and  $C_B$ , in our example, are in  $\mathbb{R}^3$  (for a Glass network in  $\mathbb{R}^4$ ), and their images under their respective cycle maps, one can represent a point on a ray with the ray's intersection with the plane of unit  $L_1$  norm,  $y_1 + y_2 + y_3 = 1$ . Thus, the 3-dimensional returning cone is represented by a two-dimensional polygon, which is the cross section of the cone with the unit  $L_1$ -norm plane, with only the first two coordinates plotted in Figure 5.3. The image of each returning cone under its respective map,  $M_A(C_A)$  and  $M_B(C_B)$  is also depicted in Figure 5.3, showing that all points in  $C_A \cup C_B$  map back into  $C_A \cup C_B$ , which is thus a trapping region.

Thus, long term dynamics of this network (or at least the basin of attraction of this trapping region) can be represented on the subset of the TG that is just the union

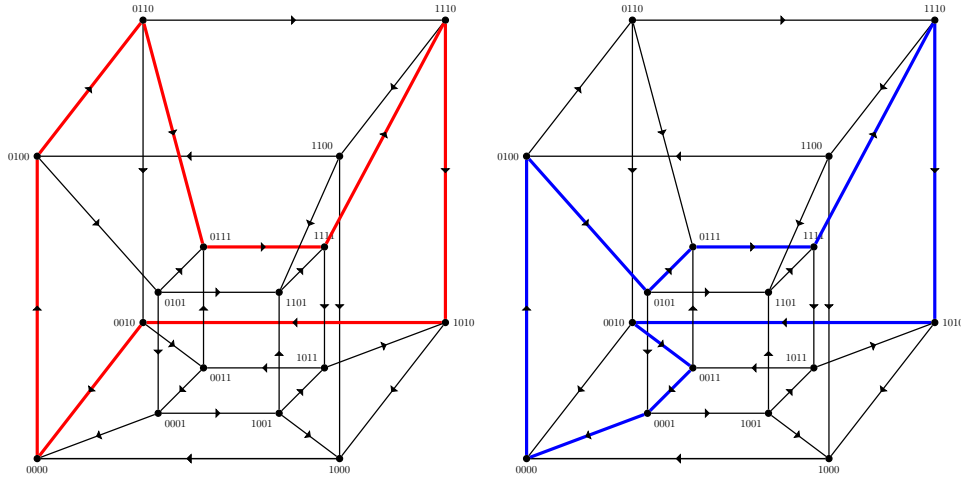


Fig. 5.4: Left: TG for the example with cycle  $A$  outlined in Red. Right: TG for the example with cycle  $B$  outlined in Blue.

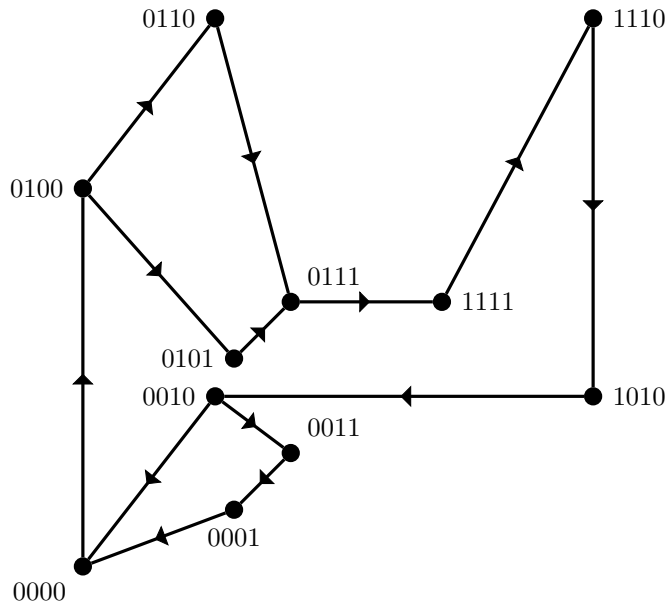


Fig. 5.5: Reduced TG for the example Glass network with only the trapping region.

of cycles  $A$  and  $B$ . Figure 5.4 shows the TG with cycles  $A$  and  $B$  outlined in red and blue respectively. Figure 5.5 shows the reduced graph,  $TG_r$ , that contains only the dynamics allowed by cycles  $A$  and  $B$ . The entropy calculated from the  $TG_r$ 's adjacency matrix is  $h_{TG_r} \approx 0.224$ , about one quarter the entropy of the original TG. However there are still significant improvements that can be made to the upper bound, by taking into account more information on the dynamics. The  $TG_r$  contains 4 cycles, not just  $A$  and  $B$ , and so includes dynamics not allowed in the trapping

region. Additionally, it can be seen in Figure 5.3 that the cycle sequence  $BB$  is forbidden, since  $M_B(C_B) \cap C_B = \emptyset$ . In other words, after a circuit of cycle  $B$ , the next cycle must be  $A$ , since  $M_B(C_B) \subset C_A$ . This suggests that while our upper bound calculated from the  $TG_r$  is a significant improvement over the original TG, further refinements can be made to obtain an even lower upper bound on entropy.

**6. Further Refinements.** In this section, a procedure is developed to obtain tighter upper bounds on entropy by eliminating cycles and sequences of cycles that are shown to be impossible or transient in computations of returning regions and their images. The key idea is *state splitting*. As well as single cycles, sequences of cycles may also be forbidden. State splitting can be used to remove cycle sequences of arbitrary length, thus allowing for more accurate graph representations of the underlying dynamics.

**6.1. State Splitting of  $TG_r$ .** In the example of the previous section, the reduced graph,  $TG_r$ , is the union of cycles  $A$  and  $B$ , which have many nodes and edges in common, but separate in two places. As a result, the graph contains two additional cycles,  $C$  and  $D$ , that do not occur in the trapping region, each of which combines part of cycle  $A$  with part of cycle  $B$ :

$$C : 1110 \rightarrow 1010 \rightarrow 0010 \rightarrow 0000 \rightarrow 0100 \rightarrow 0101 \rightarrow 0111 \rightarrow 1111$$

$$D : 1110 \rightarrow 1010 \rightarrow 0010 \rightarrow 0011 \rightarrow 0001 \rightarrow 0000 \rightarrow 0100 \rightarrow 0110 \rightarrow 0111 \rightarrow 1111$$

In fact, the returning cones for cycles  $C$  and  $D$  are empty. (Technically, the boundary between the returning cones for cycles  $A$  and  $B$  is the returning cone for both cycles  $C$  and  $D$ , but this has no interior as a set in  $\mathbb{R}^3$ . Trajectories from these points pass through simultaneous switching points where the box sequence of the cycle is not precisely defined, so these points do not in any case belong to  $\mathcal{D}$  or  $\mathcal{D}_{TR}$ ). Thus, it is impossible for trajectories to follow cycle  $C$  or  $D$  and a further modification of the  $TG_r$  that reflects this fact will further improve our upper bound on entropy.

Returning cones on a starting wall are distinct; they do not overlap, apart from potentially sharing a boundary (which is not in  $\mathcal{D}$  or  $\mathcal{D}_{TR}$ ). Thus, there are disjoint subsets of  $\mathcal{D}_{TR}$  in each wall uniquely identified with a particular cycle. In general, there may also be subsets that do not return to the starting wall, which are excluded from consideration. This gives a natural way to define a state splitting of the  $TG_r$  that accounts for each cycle. Every vertex on the  $TG_r$  that belongs to more than one cycle can be separated into multiple vertices, one corresponding to each cycle. Edges must be included to reflect the dynamics of the cycles, that is, to correspond to subsets of walls (subsets of  $\mathcal{D}_{TR}$ ) belonging to each cycle. Thus, vertices and edges will no longer correspond to entire boxes and walls, but to subsets of boxes and subsets of walls associated with particular cycles.

Up to this point we have exclusively dealt with one-sided shift spaces. The notions of state splitting that we need are defined for two-sided shift spaces by Lind and Marcus [28] and thus cannot be directly applied to our situation. However, we can use the natural extension of a one-sided shift space, defined as follows [13]:

**DEFINITION 6.1.** *For a given one-sided shift space  $X$ , the natural extension  $\widehat{X}$  is the space of bi-infinite sequences such that  $x \in \widehat{X}$  if and only if every sub word of  $x$  is an element in the language of  $X$ .*

The  $TG_r$  has the convenient property that for any two nodes, there exists a path connecting them. As a result, the  $TG_r$  language,  $\mathcal{L}(\mathcal{J}(TG_r)^{[2]})$ , is the same as that

of its natural extension  $\widehat{\text{TG}}_r$ , i.e.,  $\mathcal{L}(\mathcal{J}(\text{TG}_r)^{[2]}) = \mathcal{L}(\mathcal{J}(\widehat{\text{TG}}_r)^{[2]})$ , and therefore

$$h(\mathcal{J}(\text{TG}_r)^{[2]}) = h(\mathcal{J}(\widehat{\text{TG}}_r)^{[2]}).$$

For the purposes of our entropy upper bounds, we can use the natural extension to get the entropy relations we need.

Now to be precise, we reproduce here some definitions and results from the theory of symbolic dynamical systems, as in the text by Lind and Marcus [28]. First, we need some notation. For a directed graph  $G$ , with vertex (state) set  $\mathcal{V}$  and edge set  $\mathcal{E}$ , we denote the initial and terminal vertices of an edge  $e \in \mathcal{E}$  as  $i(e)$  and  $t(e)$ , respectively. For any  $I \in \mathcal{V}$ , let  $\mathcal{E}_I$  denote the set of edges starting at  $I$ , that is  $\mathcal{E}_I = \{e \in \mathcal{E} \mid i(e) = I\}$ . A state splitting is defined as follows [28, p.51]:

**DEFINITION 6.2.** *Let  $G$  be a graph with state set  $\mathcal{V}$  and edge set  $\mathcal{E}$ . For each state  $I \in \mathcal{V}$ , partition  $\mathcal{E}_I$  into nonempty disjoint sets  $\mathcal{E}_I^1, \mathcal{E}_I^2, \dots, \mathcal{E}_I^{m(I)}$ , where  $m(I) \geq 1$ . Let  $\mathcal{P}$  denote the resulting partition of  $\mathcal{E}$ , and let  $\mathcal{P}_I$  denote the partition  $\mathcal{P}$  restricted to  $\mathcal{E}_I$ . The **state split graph**  $G^{[P]}$  formed from  $G$  using  $\mathcal{P}$  has states  $I^1, I^2, \dots, I^{m(I)}$ , where  $I$  ranges over the states in  $\mathcal{V}$ , and edges  $e^j$ , where  $e$  is any edge in  $\mathcal{E}$  and  $1 \leq j \leq m(t(e))$ . If  $e \in \mathcal{E}$  goes from  $I$  to  $J$ , then  $e \in \mathcal{E}_I^i$  for some  $i$ , and we define the initial state and terminal state of  $e^j$  in  $G^{[P]}$  by  $i(e^j) = I^i$  and  $t(e^j) = J^j$ , that is,  $e^j$  goes from  $I^i$  to  $J^j$ . An **elementary state splitting of  $G$  at state  $I$**  occurs when  $m(I) = 2$  and  $m(J) = 1$  for every  $J \neq I$ .*

Roughly speaking, for each vertex that is split into multiple copies, its output edges are partitioned or split, while its input edges are duplicated, one for each copy of the vertex. If  $H = G^{[P]}$  for some partition  $\mathcal{P}$ , then  $H$  is called a **splitting** of  $G$  [28, p.54]. State splittings can be shown to be conjugate symbolic dynamical systems [28, Theorem 2.4.10, p.54]:

**THEOREM 6.3.** *If a graph  $H$  is a splitting of a graph  $G$ , then the edge shifts  $X_G$  and  $X_H$  are conjugate.*

The value of this result in what follows is that conjugate dynamical systems have the same entropy [28, Corollary 4.1.10, p.104]:

**THEOREM 6.4.** *If  $X$  is conjugate to  $Y$ , then  $h(X) = h(Y)$ .*

**COROLLARY 6.5.** *State splittings of a graph all have the same entropy as the original graph.*

The definition of a splitting,  $G^{[P]}$ , above uses a partition of the outgoing edges and is thus also called the *out-split* graph formed from  $G$  [28, p.53]. There is also a notion of in-splitting using a partition of the incoming edges [28, Definition 2.4.7, p.53], also conjugate to the original graph:

**DEFINITION 6.6.** *Let  $G$  be a graph with state set  $\mathcal{V}$  and edge set  $\mathcal{E}$ . For each state  $J \in \mathcal{V}$ , partition  $\mathcal{E}^J$  into nonempty disjoint sets  $\mathcal{E}_1^J, \mathcal{E}_2^J, \dots, \mathcal{E}_{m(J)}^J$ , where  $m(J) \geq 1$ . Let  $\mathcal{P}$  denote the resulting partition of  $\mathcal{E}$ . The **in-split graph**  $G_{[P]}$  formed from  $G$  using  $\mathcal{P}$  has states  $J_1, J_2, \dots, J_{m(J)}$ , where  $J$  ranges over the states in  $\mathcal{V}$ , and edges  $e_i$ , where  $e$  is any edge in  $\mathcal{E}$  and  $1 \leq i \leq m(i(e))$ . If  $e \in \mathcal{E}$  goes from  $I$  to  $J$ , then  $e \in \mathcal{E}_j^J$  for some  $j$ , and we define the initial state and terminal state of  $e_i$  in  $G_{[P]}$  by  $i(e_i) = I_i$  and  $t(e_i) = J_j$ .*

Our objective is to formulate a map that encodes trajectories with the separate cycles and that is consistent with a state splitting of the  $\text{TG}_r$  that does the same. Then we can remove edges that allow for impossible cycles and tighten our upper bound

on entropy. The proposed (state-split) graph can be constructed as follows. Let the edge in the  $TG_r$  corresponding to the starting wall be called the *starting edge*. Recall that all cycles under consideration pass through this edge by construction. For each of these cycles, create a copy of each of the cycle's vertices and give them a subscript indicating the cycle to which it belongs. Then, connect the vertices belonging to a given cycle by a copy of the original edges of that cycle, so that each cycle is completely separate. Then, add all possible cross edges from the copies of the initial vertex of the starting edge to the copies of the terminal vertex of the starting edge. This creates a new TG that has separate copies of all of the possible cycles allowed by the  $TG_r$ , with cross edges at the starting wall that allow for all sequences of those cycles, as allowed by the original  $TG_r$ .

The fact that this construction is conjugate to the original graph can be shown by a sequence of state-splittings. We demonstrate using our example from Section 5. There, the  $TG_r$  permits 4 possible cycles  $A$ ,  $B$ ,  $C$ , and  $D$ . The proposed state splitting shown in Figure 6.4 allows all possible cycles, but they are all separated except at the starting wall,  $(+++0)$ . It is then trivial to remove cycles  $C$  and  $D$  since they are already separated.

The sequence of out- and in-splittings necessary to transform the original  $TG_r$  into the graph representation in Figure 6.4 is as follows. We start with the original  $TG_r$  as depicted in Figure 5.5. Then, moving backwards along the flow from the starting edge, we consider edges starting at 0111. Since there is only one edge starting here, there is no partitioning to perform and the graph remains the same. Moving backwards from 0111, nodes 0110 and 0101 each have only one outgoing edge, so again there is no change to the graph structure. From both of these nodes we move backwards to the common node 0100. This node has two outgoing edges, so we perform an out-splitting as follows. We take  $\mathcal{E}_{0100} = \{(0100, 0110)^\top, (0100, 0101)^\top\}$  and create the partition  $\mathcal{P}_{0100} = \{\mathcal{E}_{0100}^1, \mathcal{E}_{0100}^2\}$ , where  $\mathcal{E}_{0100}^1 = \{(0100, 0110)^\top\}$  and  $\mathcal{E}_{0100}^2 = \{(0100, 0101)^\top\}$ . The resulting state-split graph is shown in Figure 6.1a.

Next, we move backwards to node 0000. Again, because it has multiple outgoing edges, we can partition them and perform an out-splitting. Using the edge set  $\mathcal{E}_{0000} = \{(0000, 0100^1)^\top, (0000, 0100^2)^\top\}$ , we create the partition  $\mathcal{P}_{0000} = \{\mathcal{E}_{0000}^1, \mathcal{E}_{0000}^2\}$ , where  $\mathcal{E}_{0000}^1 = \{(0000, 0100^1)^\top\}$  and  $\mathcal{E}_{0000}^2 = \{(0000, 0100^2)^\top\}$ . The resulting state-split graph is shown in Figure 6.1b. Now, performing out splittings at 0001 and 0011 using the partitions  $\mathcal{P}_{0001} = \{\mathcal{E}_{0001}^1, \mathcal{E}_{0001}^2\}$  and  $\mathcal{P}_{0011} = \{\mathcal{E}_{0011}^1, \mathcal{E}_{0011}^2\}$  respectively, where  $\mathcal{E}_{0001}^1 = \{(0001, 0000^1)^\top\}$ ,  $\mathcal{E}_{0001}^2 = \{(0001, 0000^2)^\top\}$ ,  $\mathcal{E}_{0011}^1 = \{(0011, 0001^1)^\top\}$ ,  $\mathcal{E}_{0011}^2 = \{(0011, 0001^2)^\top\}$ , and gives the state-split graphs in Figure 6.1c and Figure 6.1d respectively. Continuing, we perform 3 more out-splittings at 0010, 1010, and 1110, using the partitions  $\mathcal{P}_{0010} = \{\mathcal{E}_{0010}^1, \mathcal{E}_{0010}^2, \mathcal{E}_{0010}^3, \mathcal{E}_{0010}^4\}$ ,  $\mathcal{P}_{1010} = \{\mathcal{E}_{1010}^1, \mathcal{E}_{1010}^2, \mathcal{E}_{1010}^3, \mathcal{E}_{1010}^4\}$ ,  $\mathcal{P}_{1110} = \{\mathcal{E}_{1110}^1, \mathcal{E}_{1110}^2, \mathcal{E}_{1110}^3, \mathcal{E}_{1110}^4\}$ , respectively, where

$$\begin{aligned} \mathcal{E}_{0010}^1 &= \{(0010, 0000^1)^\top\}, \mathcal{E}_{1010}^1 = \{(1010, 0010^1)^\top\}, \mathcal{E}_{1110}^1 = \{(1110, 1010^1)^\top\}, \\ \mathcal{E}_{0010}^2 &= \{(0010, 0000^2)^\top\}, \mathcal{E}_{1010}^2 = \{(1010, 0010^2)^\top\}, \mathcal{E}_{1110}^2 = \{(1110, 1010^2)^\top\}, \\ \mathcal{E}_{0010}^3 &= \{(0010, 0011^1)^\top\}, \mathcal{E}_{1010}^3 = \{(1010, 0010^3)^\top\}, \mathcal{E}_{1110}^3 = \{(1110, 1010^3)^\top\}, \\ \mathcal{E}_{0010}^4 &= \{(0010, 0011^2)^\top\}, \mathcal{E}_{1010}^4 = \{(1010, 0010^4)^\top\}, \mathcal{E}_{1110}^4 = \{(1110, 1010^4)^\top\}. \end{aligned}$$

This produces the state-split graphs in Figure 6.1e and Figure 6.1f, and the graph in Figure 6.2 respectively.

This sequence of out-splittings produces a graph in which the only vertex with

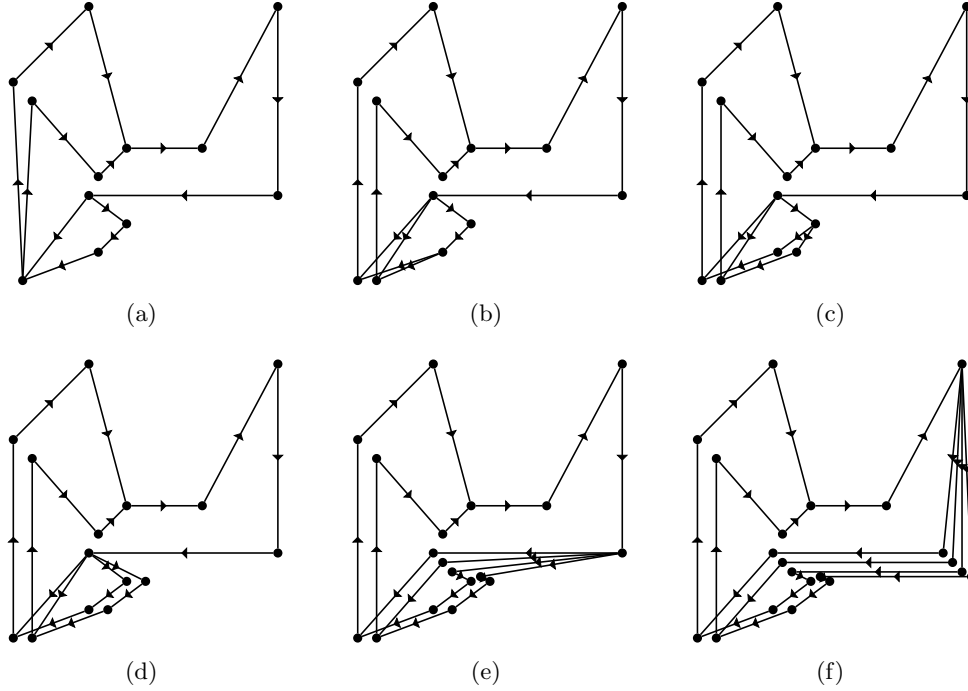


Fig. 6.1: The six sequential out splittings of the  $TG_s$  for the example Glass network

multiple outgoing edges is the initial vertex of the starting edge. To remove multiple input edges around the cycles, we perform in-splittings proceeding forward along the flow from the terminal vertex of the starting edge. Nodes  $1110^1$ ,  $1110^2$ ,  $1110^3$ , and  $1110^4$  each only have one incoming edge, so no partitioning is necessary. The same is true as we move forward along each path until two of them converge at  $0000^1$  and at  $0000^2$ . There, we can form the partitions  $\mathcal{P}_{0000^1} = \{\mathcal{E}_1^{0000^1}, \mathcal{E}_2^{0000^1}\}$  and  $\mathcal{P}_{0000^2} = \{\mathcal{E}_1^{0000^2}, \mathcal{E}_2^{0000^2}\}$ , where  $\mathcal{E}_1^{0000^1} = \{(0010^1, 0000^1)^\top\}$ ,  $\mathcal{E}_2^{0000^1} = \{(0001^1, 0000^1)^\top\}$ ,  $\mathcal{E}_1^{0000^2} = \{(0010^3, 0000^2)^\top\}$ ,  $\mathcal{E}_2^{0000^2} = \{(0001^2, 0000^2)^\top\}$ , giving the state-split graph in Figure 6.3a.

Moving forward again to  $0100^1$  and  $0100^2$ , we perform another pair of in splittings using the partitions  $\mathcal{P}_{0100^1} = \{\mathcal{E}_1^{0100^1}, \mathcal{E}_2^{0100^1}\}$  and  $\mathcal{P}_{0100^2} = \{\mathcal{E}_1^{0100^2}, \mathcal{E}_2^{0100^2}\}$ , where  $\mathcal{E}_1^{0100^1} = \{(0000_1^1, 0100^1)^\top\}$ ,  $\mathcal{E}_2^{0100^1} = \{(0000_2^1, 0100^1)^\top\}$ ,  $\mathcal{E}_1^{0100^2} = \{(0000_1^2, 0100^2)^\top\}$ , and  $\mathcal{E}_2^{0100^2} = \{(0000_2^2, 0100^2)^\top\}$ . The resulting state-split graph is depicted in Figure 6.3b. Then we perform in splittings on nodes  $0110$  and  $0101$  using the partitions  $\mathcal{P}_{0110} = \{\mathcal{E}_1^{0110}, \mathcal{E}_2^{0110}\}$  and  $\mathcal{P}_{0101} = \{\mathcal{E}_1^{0101}, \mathcal{E}_2^{0101}\}$ , where  $\mathcal{E}_1^{0110} = \{(0100_1^1, 0110)^\top\}$ ,  $\mathcal{E}_2^{0110} = \{(0100_2^1, 0110)^\top\}$ ,  $\mathcal{E}_1^{0101} = \{(0100_1^2, 0101)^\top\}$ , and  $\mathcal{E}_2^{0101} = \{(0100_2^2, 0101)^\top\}$ . This results in the state-split graph in Figure 6.3c. Then performing yet another in-splitting at  $0111$  using the partition  $\mathcal{P}_{0111} = \{\mathcal{E}_1^{0111}, \mathcal{E}_2^{0111}, \mathcal{E}_3^{0111}, \mathcal{E}_4^{0111}\}$ , where  $\mathcal{E}_1^{0111} = \{(0101_1, 0111)^\top\}$ ,  $\mathcal{E}_2^{0111} = \{(0101_2, 0111)^\top\}$ ,  $\mathcal{E}_3^{0111} = \{(0110_2, 0111)^\top\}$ ,  $\mathcal{E}_4^{0111} = \{(0110_1, 0111)^\top\}$ , gives the state-split graph in Figure 6.3d. Finally, we perform one last in-splitting at node  $1111$  using the partition of the incoming edges  $\mathcal{P}_{1111} = \{\mathcal{E}_1^{1111}, \mathcal{E}_2^{1111}, \mathcal{E}_3^{1111}, \mathcal{E}_4^{1111}\}$ , where  $\mathcal{E}_1^{1111} = \{(0111_1, 1111)^\top\}$ ,

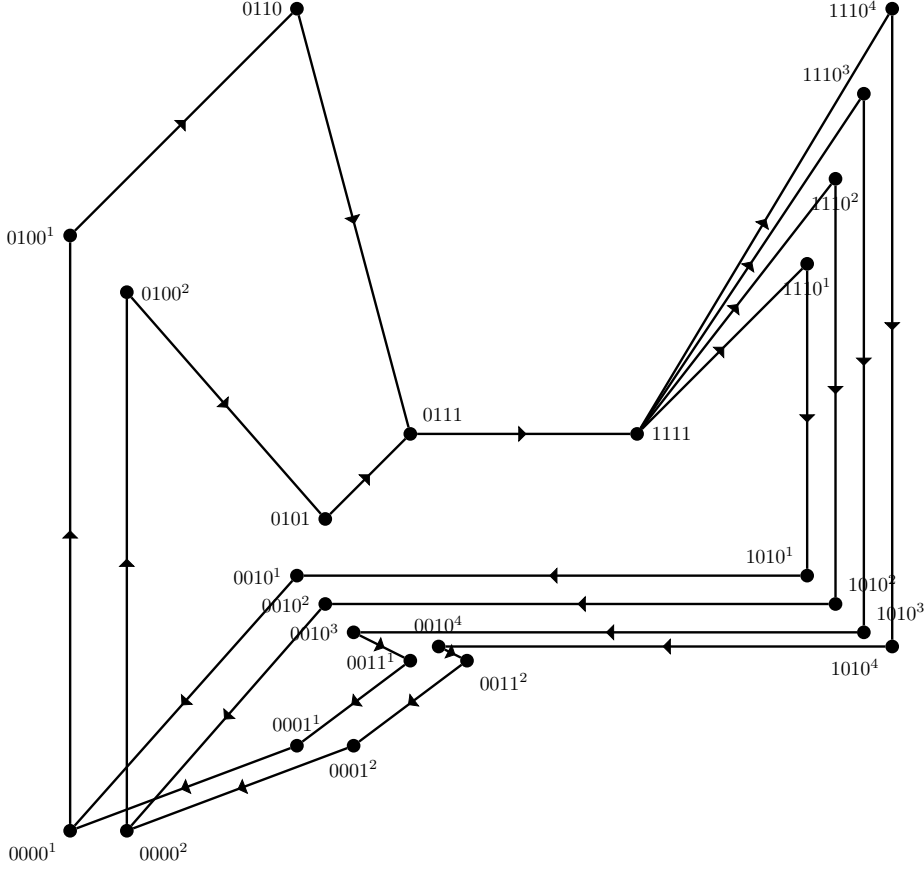


Fig. 6.2: Seventh state splitting of  $TG_r$  for the example Glass network.

$$\mathcal{E}_2^{1111} = \{(0111_2, 1111)^\top\}, \mathcal{E}_3^{1111} = \{(0111_3, 1111)^\top\}, \text{ and } \mathcal{E}_4^{1111} = \{(0111_4, 1111)^\top\}.$$

After this final in-splitting, the 4 distinct cycles on the original  $TG_r$  are completely separated, except on the starting wall, where there are cross edges that connect each of the 4 cycles. Relabeling each of the nodes to be consistent with cycle subscripts, we get the graph in Figure 6.4. Since we were able to construct this graph,  $TG_s$ , using only out-splittings and in-splittings, the natural extension is conjugate to the natural extension of the original  $TG_r$  and hence has the same entropy. Indeed the entropy calculated from Figure 6.4 is  $h \approx 0.224$ .

Since it is clear that constructing state-split graphs in this fashion does indeed lead to a conjugate system, we can now lay out the result of the general procedure, without following each step. To be precise, more notation is needed.

First we define the sets  $\mathcal{C}_A, \mathcal{C}_B, \mathcal{C}_C$ , and  $\mathcal{C}_D$  to be the sets of nodes that are followed by cycles  $A, B, C$ , and  $D$  respectively. The new alphabet for the state-split graph is  $\mathcal{A}_{ABCD} = \{a_A | a \in \mathcal{C}_A\} \cup \{a_B | a \in \mathcal{C}_B\} \cup \{a_C | a \in \mathcal{C}_C\} \cup \{a_D | a \in \mathcal{C}_D\}$ . Also define  $\mathcal{A}_A = \{a_A | a \in \mathcal{C}_A\}$ ,  $\mathcal{A}_B = \{a_B | a \in \mathcal{C}_B\}$ ,  $\mathcal{A}_C = \{a_C | a \in \mathcal{C}_C\}$ , and  $\mathcal{A}_D = \{a_D | a \in \mathcal{C}_D\}$ , the vertex sets associated with each individual cycle. The corresponding edge sets are defined as  $\mathcal{E}_S = \{(a_i, a_{i+1}) | a_i \in \mathcal{A}_S\}$  where  $S \in \{A, B, C, D\}$ . These are exactly the edges that complete each cycle loop. The cross edges that allow trajectories to follow



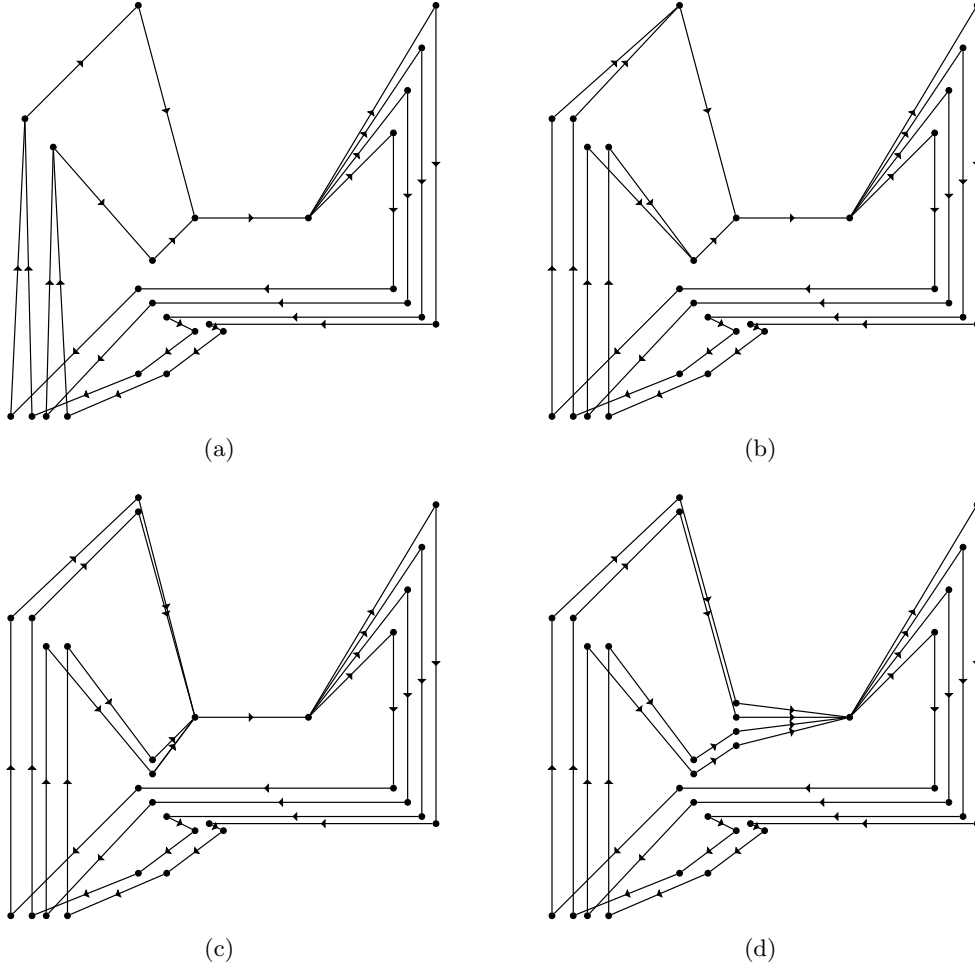


Fig. 6.3: The four sequential in-splittings of  $TG_s$  for the example Glass network.

one cycle followed by another cycle are given by the set

$$(6.1) \quad \mathcal{E}_{\text{cross}} = \bigcup_{\substack{p,q \in \{A,B,C,D\} \\ p \neq q}} \{(1111_p, 1110_q)\}.$$

The set of edges shown in Figure 6.4 is the union of these five sets:

$$(6.2) \quad \mathcal{E}_s = \mathcal{E}_A \cup \mathcal{E}_B \cup \mathcal{E}_C \cup \mathcal{E}_D \cup \mathcal{E}_{\text{cross}}.$$

For a general network that satisfies our prior conditions, the state splitting alphabet is defined similarly<sup>1</sup>. For each cycle  $\mathcal{C}_i$ , define  $\mathcal{A}_{\mathcal{C}_i} = \{a_{\mathcal{C}_i} | a \in \mathcal{C}_i\}$ , a copy of the

<sup>1</sup>If each cycle is simple, that is, no vertex is visited more than once along the cycle before returning to the starting edge, then the sequence of splittings is certainly finite. If not, in some cases it is possible to select a different starting edge from which all cycles are simple. The existence of

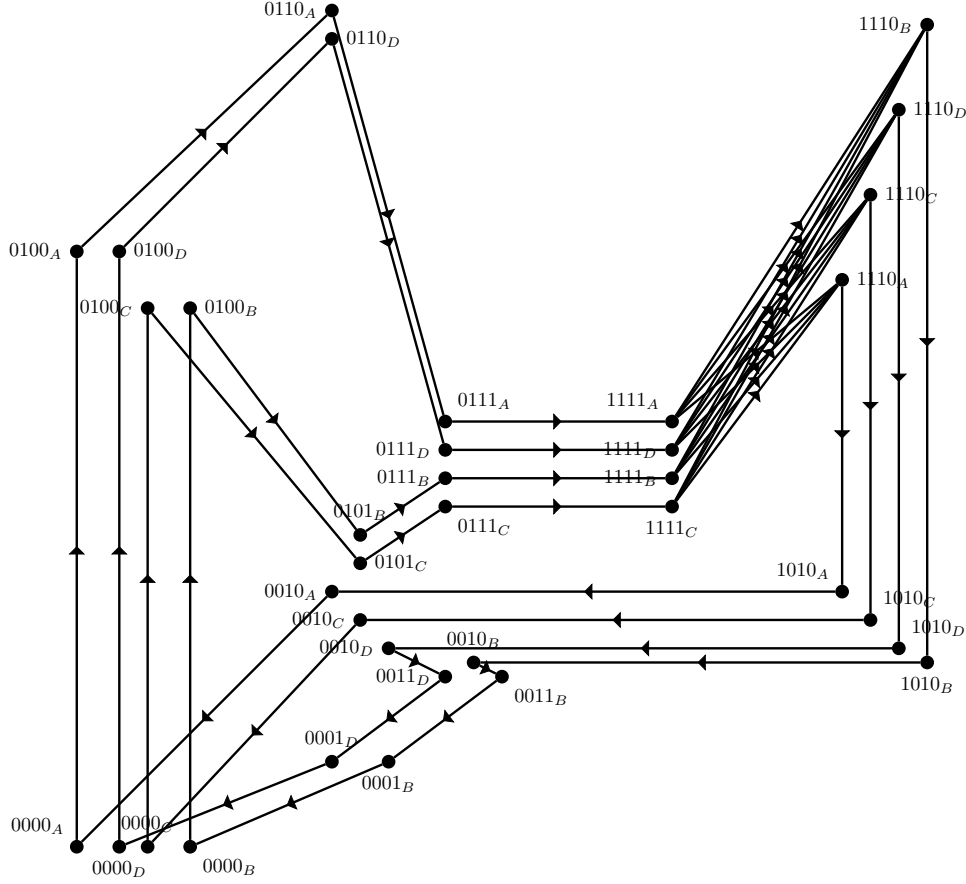


Fig. 6.4:  $TG_s$  for the example Glass network, the result of the state splitting procedure applied to  $TG_r$ .

vertex set for each cycle, using the cycle as a subscript to the vertex label. The new alphabet is defined as

$$(6.3) \quad \mathcal{A}_s = \bigcup_{i=1}^{N_c} \mathcal{A}_{C_i}.$$

The set of edges  $\mathcal{E}_s$  is also defined in the same way as in the example. First, define edges within each cycle:  $\mathcal{E}_{C_i} = \{(a_{i,j}, a_{i+1,j}) | a_{i,j} \in \mathcal{A}_{C_i}\}$ . The cross edges are defined

---

non-simple cycles, however, cannot always be avoided. Such cases may lead to the partition of the starting wall into an infinite number of cycles, but this is precluded by assumption (Condition 3). In principle, there may be non-simple cycles on the TG, which implies infinitely many cycles from and to the starting edge, but which may not imply an infinite number of cycles with non-empty returning cones. In this case, Condition 3 guarantees that there is a maximum number of times,  $k$ , that any subsidiary cycle can be traversed before returning to the starting edge such that the full cycle has a non-empty returning cone. One can stop splitting nodes in the subsidiary cycle after  $k$  times around this cycle, and the splitting procedure is still finite.

as

$$(6.4) \quad \mathcal{E}_{\text{cross}} = \bigcup_{\substack{p,q \in \{C_1, \dots, C_N\} \\ p \neq q}} \{(a_{p, \text{len}(p)}, a_{q,1})\}.$$

Note that  $\mathcal{E}_{\text{cross}}$  gives exactly the edges that start at the last node in the  $p^{\text{th}}$  cycle and connect them to the first node in the  $q^{\text{th}}$  cycle. The entire edge set for the state-splitting is

$$(6.5) \quad \mathcal{E}_s = \left( \bigcup_{i=1}^{N_c} \mathcal{E}_{C_i} \right) \cup \mathcal{E}_{\text{cross}}.$$

To verify in general that defining a new graph representation in this fashion does induce a conjugacy with the natural extension of the  $TG_r$  and gives us the entropy relation we need, we will need the following proposition

**PROPOSITION 6.7.** *For a given Glass network with starting wall  $\omega_1 \in \mathcal{E}_r$  and  $TG_r$  defined as the union of a finite number of cycles through  $\omega_1$ , define a new graph  $TG_s$ , such that*

1. *A disjoint copy of the nodes of each cycle connected by edges forming a simple chain for each cycle, apart from the starting wall,*
2. *Cross edges (at the starting wall) going from the last (terminal) node on each cycle to the first (starting) node on each cycle.*

*Then, the natural extension shift space of  $TG_s$  is conjugate to that of  $TG_r$ , and  $h_{TG_r} = h_{TG_s}$ .*

*Proof.* The procedure outlined above allows construction of  $TG_s$  from  $TG_r$  by a sequence of out-splittings node by node around the cycles followed by a sequence of in-splittings node by node around the cycles, each of which is a state-splitting by the definition of Lind and Marcus, and each of which is therefore conjugate to the preceding step. The sequence of out-splittings produces nodes (apart from the starting wall) with a single outgoing edge, and the sequence of in-splittings produces nodes (apart from the starting wall) with a single incoming edge, so the process leaves disjoint cycles apart from the starting wall. Splitting the cycles' common terminal node connects all cycles across the starting wall. Thus, the procedure produces  $TG_s$ , and it is conjugate to  $TG_r$ .

The new transition graph that separates the cycles can now be defined as  $TG_s = (\mathcal{A}_s, \mathcal{E}_s)$  and the symbolic dynamical system is analogously defined as

$$\mathcal{J}(TG_s) = \{\mathbf{a} = (a^t)_{t \in \mathbb{N}} \mid \forall t \in \mathbb{N}, (a^t, a^{t+1}) \in \mathcal{E}_s\} \subset \mathcal{A}_s^{\mathbb{N}}.$$

Since for its natural extension, the  $TG_s$  is just the result of a sequence of state-splittings of the original  $TG_r$ , and since for any two nodes on the  $TG_s$  there is a path connecting them, it follows that

$$(6.6) \quad h(\mathcal{J}(TG_r)^{[2]}) = h(\widehat{\mathcal{J}(TG_r)^{[2]}}) = h(\widehat{\mathcal{J}(TG_s)^{[2]}}) = h(\mathcal{J}(TG_s)^{[2]}). \quad \square$$

As discussed above, what is gained from this new representation of the network is the ability to remove edges to keep the TG consistent with the true dynamics. It is clear that there are no trajectories of the continuous system that follow cycles  $C$  and  $D$  in the example (they are forbidden), so one can remove those cycles from the

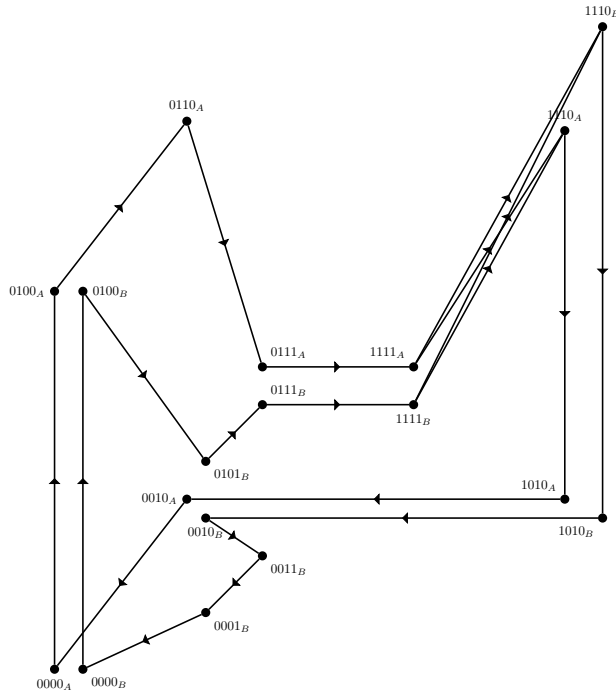


Fig. 6.5:  $TG_{sr}(1)$  for the example Glass network with cycles  $C$  and  $D$  removed.

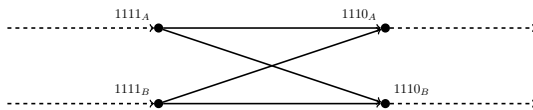


Fig. 6.6:  $TG_{sr}(1)$  for example Glass network with nodes split such that cycles  $C$  and  $D$  are removed in condensed form.

transition graph without losing any possibilities for the continuous dynamics. That is, one removes the cross edges allowing for trajectories to access cycles  $C$  and  $D$ , and the vertices and edges associated with both of those cycles. This leaves the graph,  $TG_{sr}(1)$ , in Figure 6.5, the notation anticipating further refinements. Its entropy is  $h(TG_{sr}(1)) \approx 0.111$ .

The graph in Figure 6.6 portrays the essential information in  $TG_{sr}(1)$  in a more condensed manner. After this first state-splitting, each cycle has been separated, so that when a traversal of a cycle is started, the subscript of that vertex indicates which cycle is going to be followed. Hence, if a trajectory starts on the edge between 1111B and 1110A, one knows that it came from cycle  $B$  and is next going to follow cycle  $A$ . It is sufficient to include only the vertices and edges at the starting wall since there can be no ambiguity elsewhere, as indicated by the vertex subscripts. This graph can be called the “Condensed TG”. We include the nodes and edges associated with the starting wall, and the dashed edges signify that a traversal of the cycle given by the node subscript will occur.

It is clear that the entropy of  $TG_{sr}(1)$  is less than the entropy of  $TG_r$  in our

example, or in any other example where some edges of  $\text{TG}_s$  can be removed. However, it remains to be shown that we use it as an upper bound on entropy for the “true” (continuous) dynamics. The map  $\phi$  is defined over the original alphabet and cannot distinguish between different regions on walls associated with different cycles. However, we can define a new map that does.

First, we will convert each point in space into a symbol as was done with  $\Phi$ . Let  $\{\mathcal{C}_1, \dots, \mathcal{C}_{N_c}\}$  be the set of cycles that remain in  $\text{TG}_{sr}$  after removing cycles with empty returning cones from  $\text{TG}_s$ , and let  $\mathcal{A}_{sr} \subset \mathcal{A}_s$  be the corresponding alphabet (set of nodes). We define map  $\Phi_1$ , in analogy to the original  $\Phi$ , as

$$(6.7) \quad \Phi_1(x) = (a_{c_i}, b_{c_j}) \quad \text{if} \quad x \in (\partial B_a^{\text{out}} \cap \partial B_b^{\text{in}}) \cap \mathcal{D}_{c_j}, \quad \mathcal{M}^{-1}(x) \in \partial B_a^{\text{in}} \cap \mathcal{D}_{c_i}$$

where  $i, j \in \{1, \dots, N_c\}$ . Under this definition,  $\Phi_1 : \mathcal{D}_{\text{TR}} \rightarrow \mathcal{E}_{sr}$  takes a point on a wall and identifies it with the two boxes it is between as well as indicating which cycle it is destined to follow. Again analogous to the case with  $\Phi$ , we define  $\Phi_{1\infty} : \mathcal{D}_{\text{TR}}^{\mathbb{N}} \rightarrow \mathcal{J}^{[2]}(\text{TG}_{sr}(1))$  by

$$(6.8) \quad \Phi_{1\infty}((x^k)_{k \in \mathbb{N}}) = (\Phi_1(x^k))_{k \in \mathbb{N}}.$$

Finally, composing  $\Phi_{1\infty}$  with  $\xi$  gives the map

$$(6.9) \quad \phi_1 = \Phi_{1\infty} \circ \xi : \mathcal{D}_{\text{TR}} \rightarrow \mathcal{J}^{[2]}(\text{TG}_{sr}(1)).$$

Under our conditions and on our new graph,  $\phi_1$  works exactly as  $\phi$  did, except that  $\phi_1$  differentiates between cycles;  $\phi_1(\mathcal{D}_{\text{TR}}) \subseteq \mathcal{J}^{[2]}(\text{TG}_{sr}(1))$ . Again we consider the closure to ensure that the space is indeed a shift space. So  $\overline{\phi_1(\mathcal{D}_{\text{TR}})} \subseteq \mathcal{J}^{[2]}(\text{TG}_{sr}(1))$  is the shift space of all possible trajectories, now encoded in the alphabet of  $\text{TG}_{sr}(1)$ . If we define  $h_{\phi_1(\mathcal{D}_{\text{TR}})} = h(\overline{\phi_1(\mathcal{D}_{\text{TR}})})$ ,  $h_{\text{TG}_s} = h(\mathcal{J}^{[2]}(\text{TG}_s))$  and  $h_{\text{TG}_{sr}(1)} = h(\mathcal{J}^{[2]}(\text{TG}_{sr}(1)))$ , and since  $h_{\text{TG}_s} = h_{\text{TG}_r}$ , and  $\mathcal{J}^{[2]}(\text{TG}_{sr}(1)) \subseteq \mathcal{J}^{[2]}(\text{TG}_s)$ , it follows that  $h_{\phi_1(\mathcal{D}_{\text{TR}})} \leq h_{\text{TG}_{sr}(1)} \leq h_{\text{TG}_s} = h_{\text{TG}_r} \leq h_{\text{TG}}$  where  $h_{\text{TG}_{sr}(1)}$  is the entropy of the reduced, split, reduced TG that only allows for the cycles  $A$  and  $B$ . This gives an even better upper bound on entropy.

**6.2. Arbitrary levels of refinement.** In the previous section, we showed how to remove all forbidden cycles using state-splittings. However, there may also be sequences of cycles that are forbidden. In our example, it is clear from Figure 5.3 that  $M_B(C_B) \cap C_B = \emptyset$  and hence, cycle  $BB$  is forbidden. It is easy to modify  $\text{TG}_{sr}(1)$  in Figure 6.5 to reflect this, by removing the edge between  $1111_B$  and  $1110_B$  to get Figure 6.7. This further reduction from  $\text{TG}_{sr}(1)$  allows cycle  $A$  to be followed by either  $A$  or  $B$ , but only allows cycle  $A$  to follow cycle  $B$ . This is consistent with the dynamics given by the images of the two returning cones in the trapping region and has entropy  $h \approx 0.0813$ . The condensed depiction of the graph is now given in Figure 6.8. Of course, longer sequences of cycles may also be forbidden, in general. To deal with this, we will need to further generalize the state-splitting process, the notion of a cycle and of a trapping region, beyond returning once to the starting wall as was initially considered. This will allow us to determine sequences of length  $n \in \mathbb{N}$  that are forbidden, and to show that as  $n$  increases, the entropy of these refinements converges to the entropy of the true dynamics.

A general way to identify forbidden sequences of cycles is to calculate their returning cones. Empty returning cones correspond to forbidden cycles. Returning cones for sequences of cycles, like  $AA$ ,  $AB$ ,  $BA$ , and  $BB$ , can be calculated in the same way as was done for cycles  $A$  and  $B$ .

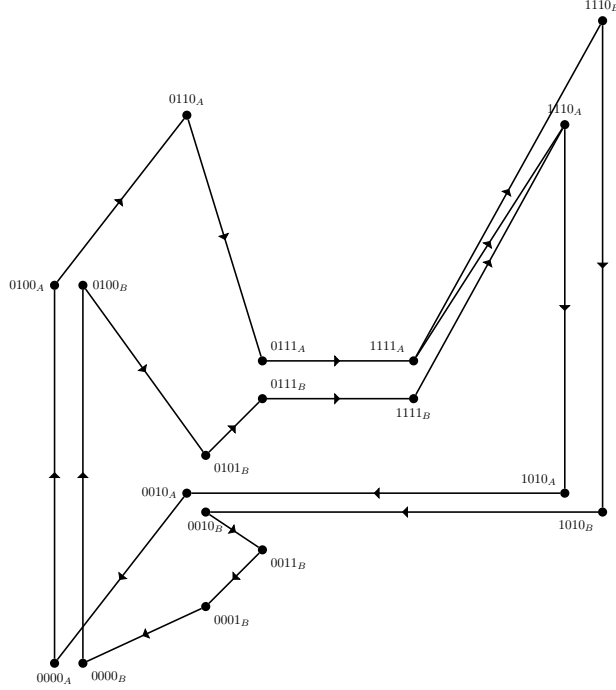


Fig. 6.7: Reduced version of  $TG_{SR}(1)$  that forbids  $BB$ .

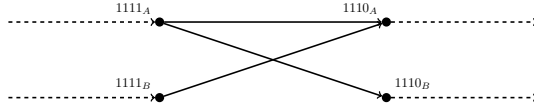


Fig. 6.8: Reduced version of  $TG_{SR}(1)$  that forbids  $BB$ , in condensed form.

To begin, we focus on a state-splitting of  $TG_{sr}(1)$  (Figures 6.5,6.6) that separates cycle sequences of length two and is consistent with the underlying dynamics. As before, in order for the state splitting to give us the correct entropy relations, we will need to consider the natural extension. Starting at the nodes  $1110_A$  and  $1110_B$ , we move from node to node forwards along each cycle performing in-splittings at each node until we get to the terminal nodes for each cycle,  $1111_A$  and  $1111_B$  respectively, where we perform the final in-splittings to obtain the graph depicted in Figure 6.9. Thus far, all two-letter combinations of cycles  $A$  and  $B$  are possible and are separated in the graph. Notice that a given cycle can only be followed by a cycle whose first letter matches the second letter of the cycle just followed. For example, cycle  $AA$  can be followed by either  $AA$  or  $AB$ , but not  $BA$  or  $BB$ . For sequences of cycles of length  $n$ , the first  $n - 1$  letters must match the last  $n - 1$  letters of the previous cycle. For example, the sequence  $BAAB$  can only be followed by cycles whose subscript starts with  $AAB$ . This rule is a consequence of in-splitting and ensures the conjugacy needed in order to compare entropy.

At the level of the  $TG_{sr}(n)$  refinement, this is the method of splitting that is required in order to separate cycle sequences of length  $n + 1$ . Since each cycle is

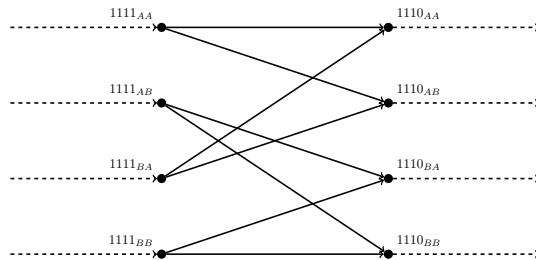


Fig. 6.9: Splitting of the  $TG_{sr}(1)$  for the example Glass network, condensed form.

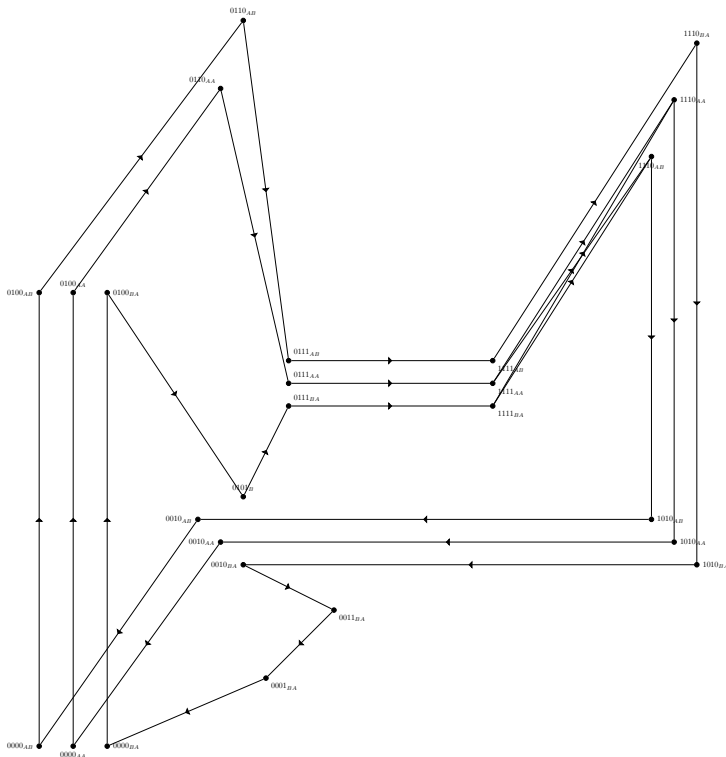


Fig. 6.10:  $TG_{sr}(2)$  for the example Glass network.

just a simple loop in the graph without branchings, to separate the cycle sequences of length  $n + 1$ , we need only perform in-splittings at each node starting with the starting node of each cycle, and moving forward along each loop, until reaching the terminal node where the final in-splitting is performed. Then edges can be removed for cycle sequences with empty returning cones. The proof that each such splitting is indeed a conjugacy follows closely the proof of Proposition 6.7.

It is clear from Figure 6.9 that in order to forbid the sequence  $BB$ , all edges to or from nodes with subscript  $BB$  must be removed. Doing so gives  $TG_{sr}(2)$ , whose full graph is shown in Figure 6.10, and condensed graph in Figure 6.11. The entropy of this graph is the same as that of the alternative reduction to forbid  $BB$  in Figure 6.7,

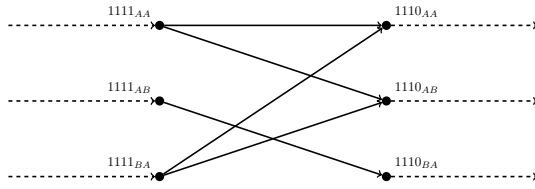


Fig. 6.11:  $TG_{sr}(2)$  for the example Glass network, condensed form.

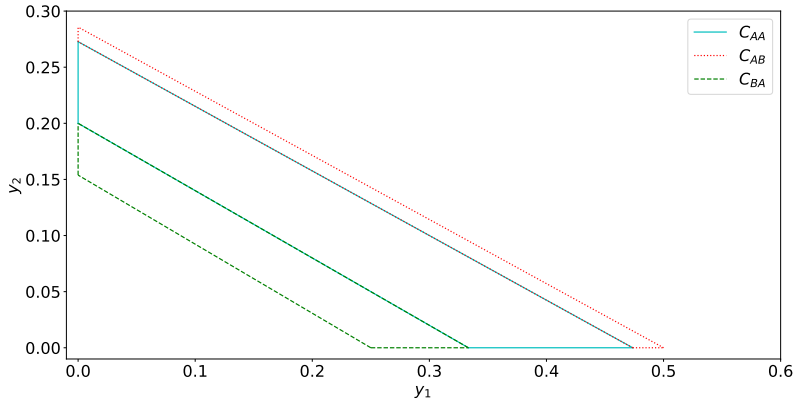


Fig. 6.12: Returning Cones for  $AA$ ,  $AB$ ,  $BA$ , and  $BB$ .

with  $h \approx 0.0813$ . It is easy to see that  $TG_{sr}(2)$  is actually just a state splitting of Figure 6.7, so the shift spaces are conjugate.

In order to construct the appropriate symbolic dynamics for the state-split graph in which sequences of cycles are separated, we will consider the returning cones for these cycle sequences, that is the sets of points from which such a cycle sequence is followed. Figure 6.12 depicts the returning cones in the starting wall for each cycle sequence of length two in our example. Note that cycle sequence  $BB$  has an empty returning cone: there is no point on the starting wall from which the sequence  $BB$  is followed. Hence,  $BB$  is forbidden. The other three returning cones partition the trapping region: the returning cone for cycle  $A$  is partitioned here into those for cycles  $AA$  and  $AB$ , while the returning cone for cycle  $BA$  is identical to that for cycle  $B$ . This partitioning of the original returning cones allows us to encode trajectories as in Section 6.1, while making them consistent with Figures 6.10 and 6.11.

The trapping tube,  $\mathcal{D}_{TR}$ , will now be expressed as a union of cycle tubes corresponding to the returning regions of the cycle sequences. Each component of  $\mathcal{D}_{TR}$  is disjoint from the rest if we follow it only until the first return to the starting wall. That is, even though we start with a returning region for a cycle sequence, and following that sequence would entail multiple returns to the starting wall, we define the cycle tube from that returning region as the sequence of images on the walls following only the first cycle (so if the sequence is  $AB$ , for example, we only follow cycle  $A$ ). This avoids intersections of tubes that would occur if we followed them further. In



our example, the cycle tubes corresponding to each of the cycle sequences of length two are

$$\mathcal{D}_{C_i C_j} = \mathcal{D} \cap \bigcup_{i=0}^{l(C_i)-1} \mathcal{M}^i(\mathcal{R}\mathcal{C}_{C_i C_j}(\omega_1))$$

where  $C_i, C_j \in \{A, B\}$  and  $l(C_i)$  denotes the length of cycle  $C_i$ . Note that  $\mathcal{D}_{BB}$  is empty. Nevertheless,

$$(6.10) \quad \mathcal{D}_{TR} = \mathcal{D}_{AA} \cup \mathcal{D}_{AB} \cup \mathcal{D}_{BA} \cup \mathcal{D}_{BB}$$

In order to encode trajectories consistent with the graphs in Figures 6.11, 6.10, and 6.9, we need to generalize the maps  $\Phi_1$  and  $\phi_1$  from Section 6.1 to work in the same way, but for any cycle sequence of length  $n$ , as well as the cycle tube  $\mathcal{D}_C$ , when  $C$  is a sequence of cycles.

DEFINITION 6.8. *For a sequence of cycles  $C_1 \dots C_m$ , the cycle tube is given by*

$$(6.11) \quad \mathcal{D}_{C_1 \dots C_m} = \mathcal{D} \cap \bigcup_{i=0}^{l(C_1)-1} \mathcal{M}^i(\mathcal{R}\mathcal{C}_{C_1 \dots C_m}(\omega_1))$$

where  $l(C_1)$  is the length of cycle  $C_1$ , the first cycle in the sequence.

The map for sequences of length two is then defined by

$$(6.12) \quad \Phi_2(x) = (a_{c_i c_j}, b_{c_k c_l}) \quad \text{if } x \in (\partial B_a^{\text{out}} \cap \partial B_b^{\text{in}}) \cap \mathcal{D}_{c_k c_l}, \mathcal{M}^{-1}(x) \in \partial B_a^{\text{in}} \cap \mathcal{D}_{c_i c_j}$$

where  $i, j, k, l \in \{1, \dots, N_c\}$ . The arbitrary combinations of indices  $i, j, k, l$  indicate all possible combinations of cycles even if some may not be realized. Then

$$(6.13) \quad \Phi_{2_\infty}((x^k)_{k \in \mathbb{N}}) = (\Phi_2(x^k))_{k \in \mathbb{N}}$$

and

$$(6.14) \quad \phi_2 = \Phi_{2_\infty} \circ \xi : \mathcal{D}_{TR} \rightarrow \mathcal{J}^{[2]}(\text{TG}_{sr}(2)).$$

Any trajectory starting on the starting wall will be encoded by  $\phi_2$  into the two-cycle-sequence alphabet.

Now it is straightforward to remove the graph nodes and edges that are associated with empty returning cones and cycle tubes, including those on the starting wall. The resulting graph we call  $\text{TG}_{sr}(2)$ , and it clearly satisfies the string of inequalities

$$(6.15) \quad h_{\phi_2(\mathcal{D}_{TR})} \leq h_{\text{TG}_{sr}(2)} \leq h_{\text{TG}_{sr}(1)} \leq h_{\text{TG}_r} \leq h_{\text{TG}}$$

The only inequality here that requires additional justification is the relationship between  $h_{\text{TG}_{sr}(2)}$  and  $h_{\text{TG}_{sr}(1)}$ . Since both of their natural extensions have the same entropy as their one-sided counterparts, it easily follows that

$$h(\mathcal{J}(\text{TG}_{sr}(2))^{[2]}) = h(\widehat{\mathcal{J}(\text{TG}_{sr}(2))^{[2]}}) \leq h(\widehat{\mathcal{J}(\text{TG}_{sr}(1))^{[2]}}) = h(\mathcal{J}(\text{TG}_{sr}(1))^{[2]}).$$

Hence, the inequalities in (6.15) hold. Since, for the corresponding comparison at step  $n$  of our refinement process the inequalities will hold for the same reason, we will omit the mention of the natural extension. However, it is important to note that most

of the inequality relations come from the fact that the entropy of the TG one-sided systems and their natural extensions are the same and that in the case of the natural extensions, state splitting induces the conjugacy.

To generalize to the case of sequences of length  $n$  is straightforward. We define new maps:  $\Phi_n$ ,  $\Phi_{n_\infty}$ , and  $\phi_n$  like their  $n = 2$  counterparts:

$$(6.16) \quad \Phi_n(x) = (a_{c_i \dots c_j}, b_{c_k \dots c_l}) \quad \text{if } x \in (\partial B_a^{\text{out}} \cap \partial B_b^{\text{in}}) \cap \mathcal{D}_{c_k \dots c_l}, \mathcal{M}^{-1}(x) \in \partial B_a^{\text{in}} \cap \mathcal{D}_{c_i \dots c_j}$$

where  $i, j, k, l \in \{1, \dots, N_C\}$ . Again, the arbitrary combinations of indices  $i, j, k, l$  indicate all possible cycles combinations of length  $n$ , even if some may not be realized.

$$(6.17) \quad \Phi_{n_\infty}((x^k)_{k \in \mathbb{N}}) = (\Phi_n(x^k))_{k \in \mathbb{N}},$$

$$(6.18) \quad \phi_n = \Phi_{n_\infty} \circ \xi : \mathcal{D}_{\text{TR}} \rightarrow \mathcal{I}^{[2]}(\text{TG}_{sr}(n)).$$

The level  $n$  state splitting is formulated in exactly the same way as the level 2 state splitting and will be denoted  $\text{TG}_{sr}(n)$ . For each  $n - 1$  length cycle sequence, create a copy associated to each appropriate length  $n$  sequence. After calculating all of the returning cones for the length  $n$  cycle sequences, remove all the nodes and edges associated with empty returning cones, including the cross edges on the starting wall associated with forbidden words. This edge shift associated with the level  $n$  refinement of the graph is again conjugate to that of the level  $n - 1$  graph by way of the properties of state splitting discussed previously.

Finally, all of this leads to the string of inequalities

$$(6.19) \quad h_{\phi_n(\mathcal{D}_{\text{TR}})} \leq h_{\text{TG}_{sr}(n)} \leq \dots \leq h_{\text{TG}_{sr}(2)} \leq h_{\text{TG}_{sr}(1)} \leq h_{\text{TG}_r} \leq h_{\text{TG}},$$

which tells us that we can refine the TG to remove dynamics associated with a forbidden cycle sequence (one with an empty returning cone) of any length we wish, and we can still use its entropy as an upper bound on the entropy of the true dynamics.

REMARK 1. *Since the adjacency matrices are sparse, computation of the eigenvalues is reliable for large  $n$ . This gives us a practical method of estimating the entropy of a network attractor to any arbitrary level of refinement, in principle.*

**6.3. The limit of the refinement process.** The following theorem states that in the limit as  $n$  goes to infinity, the entropy of the  $n^{\text{th}}$  state splitting will converge to the entropy of the true dynamics. For the proof, we will need the following proposition [28, p.123] proven by Lind and Marcus:

PROPOSITION 6.9. *Let  $X_1 \supseteq X_2 \supseteq X_3 \dots$  be shift spaces whose intersection is  $X$ . Then  $h(X_k) \rightarrow h(X)$  as  $k \rightarrow \infty$ .*

THEOREM 6.10. *For a given Glass network,  $\lim_{n \rightarrow \infty} h_{\text{TG}_{sr}(n)} = h_{\phi(\mathcal{D}_{\text{TR}})}$ .*

*Proof.* Consider the sequence of shifts of finite type  $X_{\mathcal{F}_k}$  with sets of forbidden blocks  $\mathcal{F}_k$ , given by  $\mathcal{F}_k = \{C_1 \dots C_k \mid \mathcal{R}\mathcal{C}_{C_1 \dots C_k}(\omega_1) = \emptyset\}$ . From the definition of  $X_{\mathcal{F}_k}$ , it is clear that

$$\bigcap_{k=1}^{\infty} X_{\mathcal{F}_k} = \overline{\phi(\mathcal{D}_{\text{TR}})}$$

and that  $\text{TG} \supseteq \text{TG}_r \supseteq X_{\mathcal{F}_1} \supseteq X_{\mathcal{F}_2} \supseteq X_{\mathcal{F}_3} \dots$ . So by Proposition 6.9 it follows that

$$(6.20) \quad \lim_{n \rightarrow \infty} h(X_{\mathcal{F}_k}) = h(\overline{\phi(\mathcal{D}_{\text{TR}})}) = h_{\phi(\mathcal{D}_{\text{TR}})}.$$

Now, for the given Glass network consider its  $\text{TG}_{sr}(n)$  and the mappings

$$\psi_n : \mathcal{J}^{[2]}(\text{TG}_{sr}(n)) \rightarrow \mathcal{J}^{[2]}(\text{TG})$$

where  $\psi_n$  is just the mapping that removes cycle subscripts from symbols, effectively encoding trajectories from the split alphabet into the original alphabet. From the definition of  $\psi_n$ , it is clear that it is a sliding block code and that it is finite-to-one. Additionally, as detailed by Lind and Marcus [28, p.276], finite-to-one codes on any shift space preserve entropy. So, it follows that

$$h(\mathcal{J}^{[2]}(\text{TG}_{sr}(n))) = h(\psi_n(\mathcal{J}^{[2]}(\text{TG}_{sr}(n)))).$$

Furthermore, it follows that  $\psi_n(\mathcal{J}^{[2]}(\text{TG}_{sr}(n))) = X_{\mathcal{F}_n}$ , and hence

$$h(\mathcal{J}^{[2]}(\text{TG}_{sr}(n))) = h(\psi_n(\mathcal{J}^{[2]}(\text{TG}_{sr}(n)))) = h(X_{\mathcal{F}_n}).$$

So, we have that  $h_{\text{TG}_{sr}(n)} = h(X_{\mathcal{F}_n})$  for all  $n \in \mathbb{N}$ . Finally, by Equation (6.20) it follows that  $\lim_{n \rightarrow \infty} h_{\text{TG}_{sr}(n)} = h(\overline{\phi(\mathcal{D}_{TR})})$ .  $\square$

Since it is easy to compute the entropy of  $\text{TG}_{sr}(n)$  for any  $n$ , Theorem 6.10 allows us to find an upper bound as close to the true entropy as desired.

**7. Numerical Estimation.** Here, we numerically simulate our example network and extract the number of blocks from long trajectories to get estimates of the entropy as a check on the results of our refinements above. Numerical integration is done here simply by computing the wall-to-wall maps as a discrete process from a given initial point on the starting wall.

**7.1. Have we found all of the blocks?.** It is reasonable to expect that if we simulate many trajectories from different random initial conditions, we may be able to generate all the elements of  $\mathcal{B}_n(\overline{\phi(\mathcal{D}_{TR})})$  for reasonably large  $n$ . This is easy to verify for small  $n$  since it is simple to calculate all the returning regions and the necessary trajectories are short. We experimented with blocks of length  $n = 50$ , where  $10^5$  steps (wall-to-wall transitions) seemed to generate most of the blocks (the count appeared to have stopped increasing), but a longer simulation showed that after about  $10^8$  steps there was another jump in the number of blocks. This is likely due to a few blocks of length 50 having very narrow returning cones and thus not occurring often. Increasing the trajectory length did not cause any more increases up to  $10^9$  steps. Of course, we do not know for certain if there are additional blocks of length 50 or not, without calculating the returning regions of each possible block of length 50 and checking to see which are empty, but for large  $n$  that exhaustive check is computationally prohibitive. This experiment suggested that  $10^9$  steps might be sufficient to get a good estimate of entropy for  $n$  somewhat larger than 50. In Figure 7.1 we plot the number of blocks of length 120 found in simulations of length up to  $10^9$  transitions (with the number of transitions plotted on a logarithmic scale). It is clear that the number of blocks continues to increase until about  $10^8$  steps. There are additional small jumps before about  $1.5 \times 10^8$ , but no further visible increases from there until  $10^9$  steps. If additional increases occur for larger  $n$ , their impact on entropy should be small, since that involves taking the logarithm of the number of blocks and dividing by  $n$ . Thus, we expect that for  $n \leq 120$ ,  $10^9$  transitions will give us a reasonably tight lower bound on the number of blocks. If the system is chaotic, then the number of blocks of length  $n$  continues to increase with

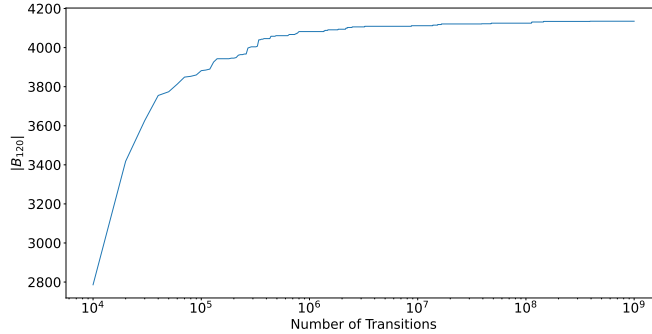


Fig. 7.1: Blocks of length 120 vs number of transitions up to  $10^9$

$n$ , and we can only estimate the number of blocks up to some finite  $n$ . The count of blocks of some particular (large) length  $n$  from a long simulation gives a lower bound on  $\mathcal{B}_n(\overline{\phi(\mathcal{D}_{TR})})$  and hence on  $\log(\mathcal{B}_n(\overline{\phi(\mathcal{D}_{TR})}))$  for that particular  $n$  and for any larger values of  $n$ , but not necessarily on the entropy, since  $\frac{1}{n} \log(\mathcal{B}_n(\overline{\phi(\mathcal{D}_{TR})}))$  may still decrease as  $n$  increases as the effects of possible longer forbidden blocks become significant. Thus, our lower bound on the number of blocks for a specific large  $n$  does not give a rigorous lower bound for the entropy.

One question that should be addressed is “what if this is just a very complicated limit cycle?”. For our example it has been proven that there is no stable limit cycle [7]. However, in general this is something that needs to be considered. It has been shown that in example networks with only 4 variables, there can be surprisingly long stable limit cycles: examples with stable limit cycles of length 174 and 252 transitions have been identified [6]. Without knowing of the existence of such long stable limit cycles ahead of time, numerical simulations would need to be long enough to identify that the number of blocks stops increasing at the length of the cycle. However, our method of upper bounds would eventually catch this, if refinement was carried far enough. If there exists a stable limit cycle involving multiple returns to a starting wall, the graph would eventually reduce to a single long loop without any branching, and which crossed the starting wall multiple times. This structure always has an entropy of 0 and hence would make numerical simulation irrelevant.

**7.2. Numerical (non-rigorous) lower bound on entropy.** For a shift space  $X$  with nonzero finite entropy,  $\mathcal{B}_n(X)$  grows approximately exponentially. For our example, it is reasonable to assume that for sufficiently large  $n$ ,  $|\mathcal{B}_n(\overline{\phi(\mathcal{D}_{TR})})| \approx a \cdot b^n$ , where  $a$  and  $b$  are positive real constants. Hence,  $h_{\phi(\mathcal{D}_{TR})} \approx \log b$ . Thus for chaotic systems, a plot of  $\log |\mathcal{B}_n(\overline{\phi(\mathcal{D}_{TR})})|$  vs  $n$  should have a linear trend, at least asymptotically. Figure 7.2 plots  $\log |\mathcal{B}_n(\overline{\phi(\mathcal{D}_{TR})})|$  against  $n$  for our example, calculated from numerically generated trajectories. The slope of the best fit line (least squares) is 0.067025, which gives an estimate of the entropy. Our second refinement from Figure 6.10 has an entropy of approximately 0.081. It is likely that there is a longer forbidden block that would only be found by refining further, so that 0.081 is an over-estimate. Alternatively, it may be that there is a very small returning cone that is visited extremely rarely, and was missed by the numerical simulation. If this is the case, then the numerical estimate of 0.067 underestimates entropy. It may

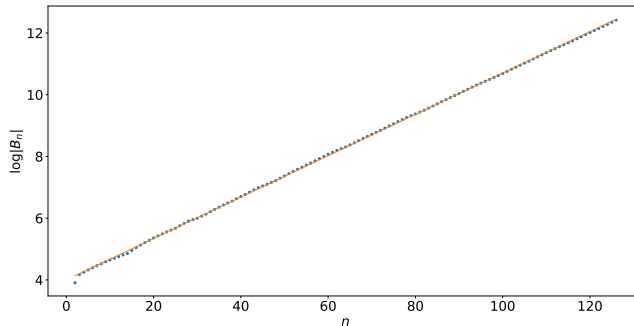


Fig. 7.2:  $\log_2$  of number of blocks of length  $n$  for  $2 \leq n \leq 126$  using a simulation of  $10^9$  transitions (dots) at each  $n$ . The solid line is the least squares best fit, which has slope  $\approx 0.0670258$ .

also be that transients occur in the numerical simulations. In the theoretical (upper-bound) estimate, transients of some length are discovered as slightly longer sequences of cycles with an empty returning cone (see above). But if the numerical simulations include a transient, they will inflate the number of blocks, and potentially lead to an over-estimate of entropy, but keep in mind that for a given trajectory, there can be at most one transient block of any given length  $n$ , so the effect on entropy is negligible for large  $n$ .

An observation from the numerical simulations is that the word  $BAAB$  does not appear in any of the generated trajectories. However, its returning cone is nonempty. It may be that  $BAAB$  is a rare sequence. The returning cone is very narrow and on the edge of the trapping region. Furthermore, the entropy of a representation that forbids  $BAAB$  is 0.0706, close to our numerical estimate of 0.067, so our numerical simulation may have missed a rare occurrence and the true entropy may be closer to 0.081. On the other hand, it may also be that every word of some length  $n > 4$  that includes  $BAAB$  is forbidden. Given that we know this system is chaotic (or at least, aperiodic), the upper bound of 0.081 may be sufficient. While 0.067 is not a rigorous lower bound, it seems likely that the actual entropy is larger than this. The numerical estimate, 0.067 and the theoretical upper bound, 0.081, are significantly closer in value than any of the first three estimates of 0.88, 0.224, and 0.111 from the TG,  $TG_r$  and  $TG_{sr}(1)$  respectively. Additionally, the upper bound 0.081 was achieved with very little work. In general, the refinement process may require more effort, but the process is simple to implement.

**8. Conclusions.** We have shown how to improve on the result of Farcot [11], which allows for the entropy of the dynamics of a Glass network to be bounded above by that of a symbolic dynamical system based on the TG. If one uses more information about the dynamics of such a network, by means of returning cones of cycles and trapping regions, one can construct discrete representations that more faithfully represent the dynamical possibilities, and thus give a tighter upper bound on entropy. The method uses structural changes by way of state splitting in the TG and removing edges that correspond to unrealizable trajectories. The procedure can be taken to an arbitrary level of precision, giving a sequence of shift spaces that have

decreasing entropy, and which we show approach the true entropy in the limit. We have removed from consideration certain types of network structure that would make our procedure more difficult, in particular, networks in which one cannot avoid an infinite number of cycles on any starting wall, or at least a potentially infinite number based on the TG alone. It might be possible to extend our work to include such examples. However, the remaining class of networks is large and dynamically diverse, with many good candidates for designs of TRNGs.

It should be noted that one could, in principle, avoid our state-spitting procedure, and simply identify forbidden sequences in the original alphabet that correspond to forbidden sequences of cycles, or even sequences of boxes that don't necessarily correspond to full cycles. This would avoid the need for defining larger and larger alphabets on the state-split graphs. However, the information about the dynamics we have comes from returning cones for cycles and trapping regions on a starting wall, and this is the information we use to identify forbidden cycles or sequences of cycles, so it is natural to structure our symbolic dynamics around them. Additionally, the state-split graphs have the advantage of allowing simple calculation of the entropy via the Perron eigenvalue of the graph's adjacency matrix.

As mentioned throughout, Glass networks have been proposed as TRNGs. Randomness in a TRNG comes mainly from thermal noise, but the strength of the idea of an underlying chaotic (deterministic) circuit design is that there is already positive entropy even without the thermal noise. The entropy of a physical realization will not be exactly the entropy of the idealized chaotic system, but whatever results from adding thermal noise to it. In a physical implementation of a TRNG, one would have to address the issue of sampling. It is desirable to extract a sequence of bits at regular time intervals, rather than transition times, for example, in order to take advantage of the phase drift caused by the physical random perturbations. However, the sampling rate will affect the entropy of the extracted bit sequences (entropy should generally increase with a decreasing sampling rate), and translating our entropy estimate based on box transitions into that of sampled bits is a non-trivial task. One expects, though, that higher entropy of the box-transition dynamics will allow higher entropy of an appropriately sampled bit sequence.

We have assumed throughout that we have a minimal trapping region. However, it may be beneficial in random number generation to consider systems with multiple disjoint trapping regions in a given starting wall. In that situation, we must deal with each minimal trapping region (and thus each attractor) separately in order to use the state-splitting process detailed in section 6. In the context of generating random numbers, one could then identify suitable initial conditions to exploit the attractor with the highest entropy. However, there may be an additional benefit to multiple trapping regions if the random "jitter" from thermal noise allows a network to jump back and forth between attractors, providing an additional source of randomness. It should be possible to automate our method for estimating entropy by an upper bound based on dynamical information that allows refinement of the state transition graph. Given a network structure, can one automatically detect a trapping region and extract a good upper bound on entropy? This is an idea for future work.

**Acknowledgments.** This work was partially supported by a Discovery Grant to RE from the Natural Sciences and Engineering Research Council (NSERC) of Canada, and a British Columbia Graduate Scholarship to BW.

## References.

- [1] R. L. ADLER, A. G. KONHEIM, AND M. H. MCANDREW, *Topological entropy*, Transactions of the American Mathematical Society, 114 (1965), pp. 309–319, <http://www.jstor.org/stable/1994177> (accessed 2023-11-16).
- [2] P. BAYON, L. BOSUET, A. AUBERT, V. FISCHER, F. POUCHERET, B. ROBISSON, AND P. MAURINE, *Contactless electromagnetic active attack on ring oscillator based true random number generator*, in Constructive Side-Channel Analysis and Secure Design, W. Schindler and S. A. Huss, eds., Springer, Berlin, Heidelberg, 2012, pp. 151–166.
- [3] A. BERMAN AND R. PLEMMONS, *Nonnegative Matrices in the Mathematical Sciences*, Academic Press, New York, second ed., 1994.
- [4] H. L. D. S. CAVALCANTE, D. J. GAUTHIER, J. E. SOCOLAR, AND R. ZHANG, *On the origin of chaos in autonomous Boolean networks*, Philosophical Transactions of the Royal Society A, 368 (2010), pp. 495–513. Presented at the International Workshop on Delayed Complex Systems (2009).
- [5] S. N. DHANUSKODI, A. VIJAYAKUMAR, AND S. KUNDU, *A chaotic ring oscillator based random number generator*, in 2014 IEEE International Symposium on Hardware-Oriented Security and Trust (HOST), IEEE, 2014, pp. 160–165.
- [6] R. EDWARDS, *Analysis of continuous-time switching networks*, Phys. D, 146 (2000), pp. 165–199, [https://doi.org/10.1016/S0167-2789\(00\)00130-5](https://doi.org/10.1016/S0167-2789(00)00130-5), [https://doi.org/10.1016/S0167-2789\(00\)00130-5](https://doi.org/10.1016/S0167-2789(00)00130-5).
- [7] R. EDWARDS, *Chaos in neural and gene networks with hard switching*, Differential Equations Dynam. Systems, 9 (2001), pp. 187–220.
- [8] R. EDWARDS, E. FARCOT, AND E. FOXALL, *Explicit construction of chaotic attractors in Glass networks*, Chaos, Solitons & Fractals, 45 (2012), pp. 666–680, <https://doi.org/https://doi.org/10.1016/j.chaos.2012.02.018>, <https://www.sciencedirect.com/science/article/pii/S0960077912000690>. Chaos and dynamics in biological networks.
- [9] R. EDWARDS AND L. GLASS, *A calculus for relating the dynamics and structure of complex biological networks*, in Adventures in Chemical Physics, R. S. Berry and J. Jortner, eds., Advances in Chemical Physics, vol. 132, Wiley, Hoboken, 2006, pp. 585–611.
- [10] R. EDWARDS, H. T. SIEGELMANN, K. AZIZA, AND L. GLASS, *Symbolic dynamics and computation in model gene networks*, Chaos: An Interdisciplinary Journal of Nonlinear Science, 11 (2001), pp. 160–169, <https://doi.org/10.1063/1.1336498>, <https://doi.org/10.1063/1.1336498>, [https://arxiv.org/abs/https://pubs.aip.org/aip/cha/article-pdf/11/1/160/7861959/160\\_1\\_online.pdf](https://arxiv.org/abs/https://pubs.aip.org/aip/cha/article-pdf/11/1/160/7861959/160_1_online.pdf).
- [11] E. FARCOT, *Geometric properties of a class of piecewise affine biological network models*, J. Math. Biol., 52 (2006), pp. 373–418, <https://doi.org/10.1007/s00285-005-0360-4>, <https://doi.org/10.1007/s00285-005-0360-4>.
- [12] E. FARCOT, S. BEST, R. EDWARDS, I. BELGACEM, X. XU, AND P. GILL, *Chaos in a ring circuit*, Chaos: An Interdisciplinary Journal of Nonlinear Science, 29 (2019), p. 043103, <https://doi.org/10.1063/1.5079941>, <https://doi.org/10.1063/1.5079941>, [https://arxiv.org/abs/https://pubs.aip.org/aip/cha/article-pdf/doi/10.1063/1.5079941/14620197/043103\\_1\\_online.pdf](https://arxiv.org/abs/https://pubs.aip.org/aip/cha/article-pdf/doi/10.1063/1.5079941/14620197/043103_1_online.pdf).
- [13] T. FRENCH, *Follower, predecessor, and extender set sequences of  $\beta$ -shifts*, Discrete and Continuous Dynamical Systems, 39 (2019), pp. 4331–4344, <https://doi.org/10.3934/dcds.2019175>, <https://www.aims sciences.org/article/id/0826532a-9ea3-4068-b96a-4c6c56fbd514>.
- [14] Z. GALIAS, *Positive topological entropy of Chua’s circuit: A computer assisted proof*, International Journal of Bifurcation and Chaos, 7 (1996), pp. 331–349.
- [15] T. GEDEON, *Attractors in continuous-time switching networks*, Commun. Pure Appl. Anal., 2 (2003), pp. 187–209, <https://doi.org/10.3934/cpaa.2003.2.187>, <https://doi.org/10.3934/cpaa.2003.2.187>.
- [16] L. GLASS, *Classification of biological networks by their qualitative dynamics*, Journal of Theoretical Biology, 54 (1975), pp. 85–107, [https://doi.org/https://doi.org/10.1016/S0022-5193\(75\)80056-7](https://doi.org/https://doi.org/10.1016/S0022-5193(75)80056-7), <https://www.sciencedirect.com/science/article/pii/S0022519375800567>.
- [17] L. GLASS, *Combinatorial and topological methods in nonlinear chemical kinetics*, The Journal of Chemical Physics, 63 (1975), pp. 1325–1335, <https://doi.org/10.1063/1.431518>, <https://doi.org/10.1063/1.431518>, [https://arxiv.org/abs/https://pubs.aip.org/aip/jcp/article-pdf/63/4/1325/18897764/1325\\_1\\_online.pdf](https://arxiv.org/abs/https://pubs.aip.org/aip/jcp/article-pdf/63/4/1325/18897764/1325_1_online.pdf).
- [18] L. GLASS, *Combinatorial aspects of dynamics in biological systems*, in Statistical mechanics and statistical methods in theory and application (Proc. Sympos., Univ. Rochester, Rochester, N.Y., 1976), U. Landman, ed., Plenum, New York, London, 1977, pp. 585–611.

- [19] L. GLASS, *Boolean and continuous models for the generation of biological rhythms*, in Dynamical systems and cellular automata (Luminy, 1983), J. Demongeot, E. Golès, and M. Tchuente, eds., Academic Press, London, 1985, pp. 197–206.
- [20] L. GLASS AND R. EDWARDS, *Hybrid models of genetic networks: Mathematical challenges and biological relevance*, Journal of Theoretical Biology, 458 (2018), pp. 111–118.
- [21] L. GLASS AND S. A. KAUFFMAN, *The logical analysis of continuous, non-linear biochemical control networks*, Journal of Theoretical Biology, 39 (1973), pp. 103–129, [https://doi.org/https://doi.org/10.1016/0022-5193\(73\)90208-7](https://doi.org/https://doi.org/10.1016/0022-5193(73)90208-7), <https://www.sciencedirect.com/science/article/pii/0022519373902087>.
- [22] L. GLASS, T. J. PERKINS, J. MASON, H. T. SIEGELMANN, AND R. EDWARDS, *Chaotic dynamics in an electronic model of a genetic network*, J. Stat. Phys., 121 (2005), pp. 969–994, <https://doi.org/10.1007/s10955-005-7009-y>, <https://doi.org/10.1007/s10955-005-7009-y>.
- [23] A. HAJMIRI, S. LIMOTYRAKIS, AND T. H. LEE, *Jitter and phase noise in ring oscillators*, IEEE Journal of Solid State Circuits, 34 (1999), pp. 790–804.
- [24] Y. HOSOKAWA AND Y. NISHIO, *Simple chaotic circuit using CMOS ring oscillators*, International Journal of Bifurcation and Chaos, 14 (2004), pp. 2513–2524.
- [25] M. INUBUSHI, *Unpredictability and robustness of chaotic dynamics for physical random number generation*, Chaos, 29 (2019), p. 033133.
- [26] N. KUZNETSOV, O. KUZNETSOVA, G. LEONOV, AND V. VAGAITSSEV, *Analytical-numerical localization of hidden attractor in electrical Chua’s circuit*, in Information in Control, Automation and Robotics: 8th International Conference, ICINCO 2011, Revised Selected Papers, J.-L. Ferrier, G. O. Bernard, Alain, and K. Madani, eds., Springer, Berlin, Heidelberg, 2011, pp. 149–158.
- [27] Q. LI AND X.-S. YANG, *Chaotic dynamics in a class of three dimensional Glass networks*, Chaos, 16 (2006), pp. 033101, 5, <https://doi.org/10.1063/1.2213579>, <https://doi.org/10.1063/1.2213579>.
- [28] D. LIND AND B. MARCUS, *An Introduction to Symbolic Dynamics and Coding*, Cambridge Mathematical Library, Cambridge University Press, Cambridge, second ed., 2021, <https://doi.org/10.1017/9781108899727>, <https://doi.org/10.1017/9781108899727>.
- [29] Y. LUO, W. WANG, S. BEST, Y. WANG, AND X. XU, *A high-performance and secure TRNG based on chaotic cellular automata topology*, IEEE Transactions on Circuits and Systems - I: Regular Papers, 67 (2020), pp. 4970–4983.
- [30] A. T. MARKETOS AND S. W. MOORE, *The frequency injection attack on ring-oscillator-based true random number generators*, in Cryptographic Hardware and Embedded Systems - CHES 2009, C. Clavier and K. Gaj, eds., Springer, Berlin, Heidelberg, 2009, pp. 317–331.
- [31] H. MARTÍN, T. KORAK, E. S. MILLÁN, AND M. HUTTER, *Fault attacks on STRNGs: Impact of glitches, temperature, and underpowering on randomness*, IEEE Transactions on Information Forensics and Security, 10 (2015), pp. 266–277, <https://doi.org/10.1109/TIFS.2014.2374072>.
- [32] T. MATSUMOTO, *A chaotic attractor from Chua’s circuit*, IEEE Transactions on Circuits and Systems, CAS-31 (1984), pp. 1055–1058.
- [33] T. MESTL, C. LEMAY, AND L. GLASS, *Chaos in high-dimensional neural and gene networks*, Phys. D, 98 (1996), pp. 33–52, [https://doi.org/10.1016/0167-2789\(96\)00086-3](https://doi.org/10.1016/0167-2789(96)00086-3), [https://doi.org/10.1016/0167-2789\(96\)00086-3](https://doi.org/10.1016/0167-2789(96)00086-3).
- [34] D. P. ROSIN, *Dynamics of Complex Autonomous Boolean Networks*, Springer Theses, Springer Cham, Heidelberg, 2015, <https://doi.org/10.1007/978-3-319-13578-6>.
- [35] D. P. ROSIN, D. RONTANI, AND D. J. GAUTHIER, *Ultrafast physical generation of random numbers using hybrid Boolean networks*, Physical Review E, 87 (2013), p. 040902(R).
- [36] S. SRIVASTAVA AND J. ROYCHOWDHURY, *Analytical equations for nonlinear phase errors and jitter in ring oscillators*, IEEE Transactions on Circuits and Systems: I Regular Papers, 54 (2007), pp. 2321–2329.
- [37] C. TANOUGAST, *Hardware implementation of chaos based cipher: Design of embedded systems for security applications*, in Chaos-Based Cryptography, L. Kocarev and S. Lian, eds., Springer, Berlin, Heidelberg, 2011, pp. 297–330.
- [38] R. ZHANG, H. L. D. S. CAVALCANTE, Z. GAO, D. J. GAUTHIER, J. E. SOCOLAR, M. M. ADAMS, AND D. P. LATHROP, *Boolean chaos*, Physical Review E, 80 (2009), p. 045202(R).